Marine Geology
June 2019, Volume 412 Pages 1-18
https://doi.org/10.1016/j.margeo.2019.02.007
https://archimer.ifremer.fr/doc/00483/59512/

Cold-water coral mounds in the southern Alboran Sea (western Mediterranean Sea): Internal waves as an important driver for mound formation since the last deglaciation

Wang Haozhuang [1,*], Lo Iacono Claudio [2,3], Wienberg Claudia [1], Titschack Jürgen [1,4], Hebbeln Dierk [1]

[1] Center for Marine Environmental Sciences (MARUM), Bremen University, Leobener Strasse 2, 28359 Bremen, Germany
[2] National Oceanography Centre, University of Southampton, Waterfront Campus, European Way, SO143ZH Southampton, United Kingdom
[3] Marine Sciences Institute (ICM), Spanish National Research Council (CSIC), Paseo Maritimo de la Barceloneta 37-49, 08003 Barcelona, Spain
[4] Senckenberg am Meer (SAM), Marine Research Department, Südstrand 40, 26382 Wilhelmshaven, Germany

* Corresponding author : Haozhuang Wang, email address : hwang@marum.de

Abstract :

Cold-water corals (CWCs) are widely distributed in the entire Alboran Sea (western Mediterranean Sea), but only along the Moroccan margin they have formed numerous coral mounds, which are constrained to the West and the East Melilla CWC mound provinces (WMCP and EMCP). While information already exists about the most recent development of the coral mounds in the EMCP, the temporal evolution of the mounds in the WMCP was unknown up to the present. In this study, we present for the first time CWC ages obtained from four sediment cores collected from different mounds of the WMCP, which allowed to decipher their development since the last deglaciation. Our results revealed two pronounced periods of coral mound formation. The average mound aggradation rates were of 75–176 cm kyr^{-1} during the Bølling-Allerød interstadial and the Early Holocene, only temporarily interrupted during the Younger Dryas, when aggradation rates decreased to <45 cm kyr^{-1}. Since the Mid Holocene, mound formation significantly slowed-down and finally stagnated until today. No living CWCs thrive at present on the mounds and some mounds became even buried. The observed temporal pattern in mound formation coincides with distinct palaeoceanographic changes that significantly influenced the local environment. Within the Alboran Sea, enhanced surface ocean productivity and seabed hydrodynamics prevailed during the Bølling-Allerød and the Early Holocene. Only with the onset of the Mid Holocene, the area turned into an oligotrophic setting. The strong hydrodynamics during the mound formation periods are most likely caused by internal waves that developed along the water mass interface between the Modified Atlantic Water and the Levantine Intermediate Water. In analogue to observations from modern CWC settings, we assume that internal waves created turbulent hydrodynamic conditions that increased the lateral delivery of particulate material, promoting the availability of food for the sessile CWCs. Overall, our data point to the dominant role of the water column structure in controlling the proliferation of CWCs and hence the development of coral mounds in the southern Alboran Sea.

Highlights

► Coral mounds formation in southern Alboran Sea reinitiated since the onset of B/A interstadial. ► Coral mound aggradation rate reached up to 704 cm kyr^{-1}. ► Internal waves play a dominant role in controlling mound formation. ► Coral mound formation stagnated since the Late Holocene.

Keywords : Cold-water coral mounds, Coral mound formation, Mound aggradation rate, Last deglaciation, Internal waves, Levantine Intermediate Water, Alboran Sea

1. Introduction

Scleractinian framework-forming cold-water corals (CWCs) show a world-wide distribution and form important deep-sea ecosystems providing habitats for numerous marine organisms (e.g., Henry and Roberts, 2007; Roberts et al., 2009). The most prominent species *Lophelia pertusa* and *Madrepora oculata* tolerate a wide range of physico-chemical conditions in the ocean, with temperature, salinity, dissolved oxygen concentrations, pH, aragonite saturation, and water mass density being the most important properties of the surrounding water masses that influence their occurrence (e.g. Freiwald et al., 2002; Davies et al., 2008; Dullo et al., 2008; Davies and Guinotte, 2011; Flögel et al., 2014; Büscher et al., 2017). However, the proliferation of CWCs is even more controlled by the availability of sufficient food (phytoplankton, zooplankton, particulate organic material), which is steered by enhanced surface productivity and/or the local hydrodynamic regime (including geostrophic currents, internal tides and waves, cascading and down-welling processes), providing periodic to constant delivery of sufficient food particles (White et al., 2005; Mienis et al., 2007; Duineveld et al., 2007; Davies et al., 2009; Duineveld et al., 2012; Taviani et al., 2016).

Over geological timescales, the sustainable growth of CWCs can shape the seabed topography along the continental margins by forming three-dimensional structures, named coral mounds (Roberts et al., 2009; Wienberg and Titschack, 2017; Lo Iacono et al., 2018). In the Atlantic, coral mounds are usually found at water depths between 200 and 1000 m and are often arranged as clusters or coral mound provinces consisting of hundreds to thousands of mounds (e.g. De Mol et al., 2002; Fosså et al., 2005; De Haas et al., 2009; Correa et al., 2012; Glogowski et al., 2015; Vandorpe et al., 2017; Hebbeln et al., 2019). Individual mounds have oval to elongated shapes, and appear as ridge-like structures, which extend over hundreds to thousands of metres (Wheeler et al., 2007). The height of individual mounds varies from a few to hundreds of metres (e.g., Van Weering et al., 2003; Mienis et al., 2007; Wheeler et al., 2007; Collart et al., 2018).

Although food delivery plays a crucial role in the proliferation of CWCs, the formation of coral mounds is even more sensitive to the complex interplay between the sustained growth of CWC, their baffling capacity and sediment supply that eventually result in the formation of coral mounds (Wheeler et al., 2005; Huvenne et al., 2009; Mienis et al., 2009; Titschack et al., 2015; Titschack et al., 2016; Victorero et al., 2016). Consequently, coral mounds consist of coral frameworks and fragments, remains of coral associated fauna, and hemipelagic sediments. Their development can last from thousands to even millions of years (e.g., Kano et al., 2007; Frank et al., 2011;Raddatz et al., 2014). Therefore, the coral mounds provide unique archives to reconstruct the palaeoceanographic constraints during their formation as well as the development of CWC populations in relation to changing environments.

Studies from various coral mound provinces in the NE Atlantic revealed distinct temporal patterns of mound formation which appear to be closely related to climate changes, such as those induced by glacial-interglacial variability (e.g., Kano et al., 2007; Frank et al., 2011). On a regional scale, mound formation is controlled by strong near-bottom hydrodynamics and enhanced paleo-productivity (Dorschel et al., 2005; Rüggeberg et al., 2007; Wienberg et al., 2010; Eisele et al., 2011; Matos et al., 2015), while low dissolved oxygen concentrations might hinder the development of coral mounds (Wienberg et al., 2018). Moreover, the water column structure and water mass circulation at intermediate water depths seem to play an important role in stimulating or suppressing the formation of coral mounds (White and Dorschel, 2010; Raddatz et al., 2014; Matos et al., 2017; Wienberg et al., 2018). Nevertheless, our knowledge about environmental parameters and their complex interplay controlling coral mound formation is still limited.

In the Mediterranean Sea, coral mounds are mainly found along the Moroccan margin, in the southern Alboran Sea, where they are constrained to two coral mound provinces 35 km northwest and 15 km northeast of the Spanish enclave Melilla (Cape Tres Forcas; Fig. 1). Within the West Melilla CWC mound province (WMCP), more than 100 oval to elongated coral mounds occur in two clusters at water depths of 300-430 m (Fig. 1; Lo Iacono et al., 2014). They have diameters of 50-476 m, and arise 8-21 m above the seafloor. In addition, few isolated circular coral mounds with heights of 10-35 m were found in water depths of 450-590 m (Fig. 1). Today, no living CWCs are observed on the mounds of the WMCP, and some of the mounds are partly buried (Lo Iacono et al., 2014). The East Melilla CWC mound province (EMCP) displays different morphologies and dimensions of mounds. In the north, three very steep ridges occur at water depths of 250-450 m, which have heights of 50-150 m and stretch from 3 km to almost 20 km in length (Brittlestar ridges I, II and III; Hebbeln, 2019). To the south, more than 40 oval to arcuate coral mounds (height: 20-40 m) and partly buried elongated ridges (height: 10 m) occur at water depths of 200-300 m (Comas et al., 2009; Hebbeln, 2019). Spotted colonies of living CWCs have been observed on the Brittlestar ridges and on some of the smaller mounds, displaying a rather sparse distribution (Hebbeln et al., 2009; Fink et al., 2013).

Recent studies provided some first information on the temporal development of the CWCs and coral mounds in the EMCP during the past 14 kyr. CWCs experienced marked proliferation during the late Bølling-Allerød (B/A) interstadial and the Early Holocene, associated with high mound aggradation rates (ARs) of 140-420 cm kyr^{-1} (Fink et al., 2013; Stalder et al., 2015). These two periods of pronounced mound formation contrast with a period of nearly stagnation, coinciding with the Younger Dryas (YD), when ARs decreased to 30-50 cm kyr^{-1}. Since the late Early Holocene, CWC growth was reduced and coral mound formation significantly slowed down until present (Fink et al., 2013; Stalder et al., 2015). Overall, it is assumed that coral mound formation in the EMCP is controlled by a variable set of environmental parameters such as sea surface and export productivity, strong hydrodynamics, and bottom water oxygenation, which in turn seem to be steered by changes in the water column structure (Fink et al., 2013; Stalder et al., 2015). So far, nothing is known about the timing of CWC growth and coral mound formation in the WMCP. Based on seismic data, it is assumed that a simultaneous initial CWC colonisation took place in the WMCP and that some of the mounds became buried concurrent to the effects of sea-level rise that likely induced changes in near-bottom hydrodynamics and sedimentation rates on the slope (Lo Iacono et al., 2014). However, no temporal framework for the evolution of the coral mounds in the WMCP has been established so far, mainly due to the lack of sediment cores collected in this region.

The main aims of this study are therefore (i) to reconstruct the temporal development of coral mounds in the WMCP, and (ii) to relate the derived temporal patterns in mound formation to changes in the regional environmental setting. For this purpose, coral-bearing (on-mound) cores were collected from different coral mounds in the WMCP, and complemented by one off-mound sediment core (barren of any coral fragments) retrieved close to the studied mounds. The on-mound cores were described and dated to elucidate the local coral mound formation pattern, while the off-mound core was used for multi-proxy analyses to assess the (palaeo-) environmental controls on mound development. Furthermore, we evaluated any differences in mound evolution between the WMCP and the EMCP, and addressed the decisive role of water mass circulation, in particular distinct processes at water mass boundaries, as a crucial local factor driving the development of coral mounds in the southern Alboran Sea.

2. Regional Setting

The Alboran Sea is located at the westernmost part of the Mediterranean Sea, and is connected to the Atlantic Ocean through the Gibraltar Strait (Fig. 1). The oceanography of the Alboran Sea is characterized by three different water masses, the Modified Atlantic Water (MAW), the Levantine Intermediate Water (LIW) and the Western Mediterranean Deep Water (WMDW). The MAW, formed by the mixing of Atlantic Water and the surface waters of Alboran Sea (Millot and Taupier-Letage, 2005), flows at the surface down to 150-200 m water depth (Millot, 1999). Within the Alboran Sea, the MAW forms two anti-cyclonic gyres, the quasi-permanent West and the variable East Alboran Gyres (WAG and EAG; Fig. 1), which have diameters of 100 km and reach down to 200-300 m water depth (Heburn and La Violette, 1990). Their intensity is closely related to the strength of the Atlantic Water inflow (Heburn and La Violette, 1990; Vargas-Yáñez et al., 2002). The LIW, which originates in the eastern Mediterranean Sea, flows westward beneath the MAW at depths between 200 m and 600 m. The core of the LIW is found at around 400 m water depth in the Alboran Sea indicated by the salinity maximum (Millot, 2009). Its thickness decreases gradually from the European to the African continental margin (Brankart and Pinardi, 2001; Fabres et al., 2002). The WMDW is formed in the Gulf of Lions, and spreads into the Balearic Sea and further into the Alboran Sea, where it flows westward underneath the LIW, at water depths of >600 m (Millot, 1999).

The Alboran Sea is the area with the highest productivity within the overall oligotrophic Mediterranean Sea (Morán and Estrada, 2001; D'Ortenzio and Ribera d'Alcalà, 2009;). The increased productivity is driven by locally restricted upwelling that occurs along the edge of the WAG and at the eastern limb of the EAG (Sarhan et al., 2000; Baldacci et al., 2001). The siliciclastic sediment fraction in the Alboran Sea is a mixture of aeolian dust, which is transported northward from the Sahara (Stuut et al., 2009), and fluvial input, which mainly derives from the Iberian Peninsula (Fabres et al., 2002). The only larger river along the Moroccan coast is the Moulouya River, which enters the Alboran Sea 50 km east of the EMCP.

3. Material and Methods

Within this study, four “on-mound” gravity cores retrieved from coral mounds of the WMCP and one “off-mound” gravity core collected from the adjacent seafloor were analysed (Fig. 1; Table 1). The two on-mound cores MD13-3451G and MD13-3452G were collected in 2013 during the MD194 "Gateway" Eurofleets Cruise onboard the RV Marion Dufresne (Van Rooij et al., 2013). The other two on-mound cores GeoB18127-1 and GeoB18130-1, and the off-mound core GeoB18131-1 were collected in 2014 during the MSM-36 “MoccoMebo” cruise on board the RV Maria S. Merian (Hebbeln et al., 2015). The on-mound cores have recovery lengths between 148 cm and 563 cm, and the off-mound core has a recovery length of 851 cm (Table 1).

The four on-mound cores were frozen for 24 hours to -20 °C before cutting them lengthwise with a diamond saw to secure that the sediment, consisting of coral fragments embedded in hemi-pelagic sediment, is kept intact during the opening process. The cores were described, and coral fragments were sampled at various core depths for absolute dating.

The off-mound core GeoB18131-1 was split in a conventional way into working and archive halves and was used for palaeoceanographic multi-proxy analyses.

3.1 On-mound core analyses

3.1.1 Sedimentological core description

Cores MD13-3451G and MD13-3452G were visually described to provide (qualitative, 2D) information on variations in coral content and clast size throughout the cores. The coral content was estimated based on its coverage on the cutting surface (unit: surface (surf.) %) of the core halves, and changes in CWC clast size were described (see Fig. S1 in Supplementary Material).

In contrast, the core description provided for cores GeoB18127-1 and GeoB18130-1, is based on the analyses of computer tomography (CT) scan data. These analyses were further used to define CWC preservation pattern (CPP) by quantifying coral clast size and orientation (see Table S1 in Supplementary Material) in close accordance to a CPP classification introduced by Titschack et al. (2015).

The CT scans were performed by using Toshiba Aquilion 64 computer tomography at the hospital Klinikum Bremen-Mitte (Bremen, Germany). The X-ray source voltage was 120 kV and the current was 600 mA. Images were reconstructed based on the Toshiba patented helical cone beam reconstruction technique. The CT scan resolution was 0.35 mm in x-y and 0.5 mm in z direction (0.3 mm reconstruction interval). The CT data were processed with the Zuse Institute Berlin edition of Amira software (version 2015.37; Stalling et al., 2005; http://amira.zib.de), following the method described in Titschack et al. (2015) with only minor modification(for further processing details, see Supplementary Material).

3.1.2 Radiocarbon and Uranium-series dating

A total of 38 fragments of *L. pertusa* and *M. oculata* were sampled from the four on-mound cores at various depths and used for dating. Prior to the analyses, all coral fragments were cleaned mechanically to remove cortical corrosion, bioerosion holes, and adhering detritus from the coral skeletons.

Twelve coral samples collected from cores MD13-3451G and MD13-3452G, were dated by accelerator mass spectrometry (AMS) radiocarbon (^{14}C) age determination. Prior to the measurement, the coral fragments were chemically cleaned with hydrogen peroxide. The measurements were conducted at the Poznan Radiocarbon Laboratory, Poznan, Poland. All the obtained ages were corrected for ^{13}C and a mean ocean reservoir age of 400 years. The AMS ^{14}C ages were converted to calendar years using the MARINE13 curve (Reimer et al., 2013) of the web-based CALIB 7.10 software (Stuiver and Reimer, 1993; http://calib.org/calib/calib.html) and reported as kiloyears before present (kyr BP, Present=AD 1950; Table 2).

Twenty-six coral samples from cores GeoB18127-1 and GeoB18130-1 were collected for Uranium-series dating. Before the analyses, coral fragments were cleaned mechanically according to a procedure described by Frank et al., (2004). The U-series isotope measurements were performed on a ThermoFisher iCAP-Qs inductively coupled plasma mass spectrometer (ICP-MS) at the Institute of Environmental Physics, at the Heidelberg University (IUP), Germany. The reproducibility was assessed using the international uranium standard material HU1 (Cheng et al., 2000; Frank et al., 2004; Wefing et al., 2017). U-series coral ages are reported as kyr BP (Table 3).Finally, all coral mound ARs were calculated based on the linear interpolation between the dated depths of each core (Tables. 2, 3).

3.2 Off-mound core analyses

3.2.1 Radiocarbon dating

The chronostratigraphy of the off-mound core GeoB18131-1 is based on six AMS ^{14}C dates. Therefore, around 8 mg of calcium carbonate of mixed planktonic foraminifers of the size fraction >150 µm were analysed at the Poznan Radiocarbon Laboratory, Poznan, Poland. The obtained ages were corrected as described above (Table 4).

3.2.2 Stable oxygen and carbon isotope analyses

For stable oxygen ($\delta^{18}O$) and carbon ($\delta^{13}C$) isotope measurements, the core was sampled at a 5 cm resolution. Each sample was wet-sieved and the >150 µm fraction was used to collect around 10 specimens of the two epibenthic foraminifera species: *Cibicidoides mundulus* (also described as *Cibicidoides kullenbergi*) and *Cibicidoides pachyderma*. To exclude a potential species-specific fractionation effect (vital effect) on the measured isotopic compositions of the paired samples, $\delta^{18}O$ and $\delta^{13}C$ of both species were measured separately on 16 samples.

The analyses were performed at MARUM, University of Bremen, Germany, using a Finnigan MAT 251 mass spectrometer coupled either to a Kiel I or Kiel IV automated carbonate preparation device. With a constant temperature of 75 °C, the measurements were conducted on CO_2 that evolved by phosphoric acid treatment. Ground Solnhofen limestone was used as internal standard, which has been calibrated against Vienna Pee Dee Belemnite (V-PDB) using the NBS 19 standard. The measured data were reported relative to the V-PDB standard. The analytical standard deviation for $\delta^{18}O$ and $\delta^{13}C$ was ± 0.04‰ and ± 0.03‰ for the paired samples and ± 0.06‰ and ± 0.03‰ for the mono-species samples, respectively. The $\delta^{18}O$ and $\delta^{13}C$ anomaly between the two species has a mean value of 0.04‰ and -0.04‰, respectively, with a standard deviation of less than 0.25 for both. Given the standard deviation during the measurement, our record from mixed samples is valid.

The benthic foraminifera $\delta^{18}O$ record ($\delta^{18}O_{Cib}$) was used to establish a chronostratigraphy for the off-mound core (supplemented by the AMS ^{14}C dates). The $\delta^{13}C_{Cib}$ record was applied to trace past changes in the water column structure. Epibenthic foraminifera are commonly used in palaeoceanographic studies as their tests incorporate $\delta^{13}C$ in equilibrium with the ambient water (e.g., Curry et al., 1988; Curry and Oppo, 2005; Zahn et al., 1986). However, it has been shown that *C. mundulus* and *C. pachyderma* may record lighter $\delta^{13}C$ values than those of the ambient water suggesting an occasional infaunal habitat (Schmiedl et al., 2004; Martínez-Méndez et al., 2013; Schmittner et al., 2017 and references therein).

3.2.3 Grain-size analysis

Grain-sizes were measured on the terrigenous fraction of the sediment (sampling interval: 5cm). Prior-to the analyses, the samples were chemically treated following the method of McGregor et al. (2009). Deionized, degassed and filtered water (filtered with mesh size: 0.2 µm) was used during the entire process to reduce the potential influence of air bubbles or particles within the used water. The analyses were performed in the Particle-Size Laboratory at MARUM, University of Bremen, Germany, with a Beckman Coulter Laser Diffraction Particle Size Analyzer LS 13320. The obtained results provide the grain-size distribution of individual sample from 0.04 µm to 2000 µm in 116 size classes. All provided statistic values are based on a geometric statistic. In this study, the mean grain size is used to trace changes in bottom current strength (see also Fink et al., 2013).

3.2.4 Benthic foraminifer accumulation rate

Benthic foraminifer accumulation rates (BFARs) were analysed for the upper 368 cm of the off-mound core. From the core top to 158 cm, the sampling resolution was 10 cm whereas the resolution was increased to 5 cm between 158 cm and 368 cm core depth. The bulk samples were wet sieved and the >150 µm fraction was used for benthic foraminifer counts. Each sample was split until it contained approximately 300 individuals of benthic foraminifers, and counted (Patterson and Fishbein, 1989). All counts were corrected for splits and the BFAR (unit: $x10^3$ individuals cm^{-2} kyr^{-1}) was calculated according to the equation from Ehrmann and Thiede. (1985):

$$BFAR = SR \times DBD \times foram/1000$$

BFAR: benthic foraminifer accumulation rate;

SR: Sedimentation Rate (unit: cm kyr^{-1});

DBD: Dry bulk sediment density (unit: g cm^{-3});

foram: number of foraminifers per gram in the dry bulk sample (unit: individuals g^{-1}).

Due to the linear relation between the BFAR and the organic matter flux to the seafloor, the BFAR represents an established proxy for the export productivity (e.g., Berger and Herguera, 1992).

4. Results

4.1 On-mound core description

4.1.1 Visual core description of on-mound cores MD13-3451G and MD13-3452G

For the two on-mound cores MD13-3451G and MD13-3452G, a visual core description is provided (see Fig. S1 in Supplementary Material), as CT scan data, allowing for a detailed quantitative description or determining of CPPs, are not available for these cores. Core MD13-3451G reveals CWC fragments embedded in predominantly grey muddy matrix sediments. Based on distinct variations in coral content and coral clast size, the core is subdivided into three units. The lowermost part of the core (522-460 cm core depth) exhibits relatively high coral contents of around 30-50 surf.% with generally large coral clasts of 3-5 cm. Between 460 and 190 cm core depth, the coral contents decrease to around 10-30 surf.%. The size of the coral clasts varies mainly between 1-3 cm in length, while large coral clasts of about >3 cm in length occur occasionally at core depths of 495-460 cm, 415-335 cm and 250-200 cm. In the uppermost section of the core (190 cm to core top), very low coral content of <5 surf.% comprising coral clasts of 1-2 cm in size concentrated at core depths of 180-168 cm, 85-79 cm, and 20-0 cm, while in between these intervals, no coral clasts are visible.

Core MD13-3452G contains CWC fragments throughout the core, which are embedded in olive grey muddy matrix sediments. Changes in coral content and coral clast size allowed to divide the core into three units. The lowermost three meters of the core(558-270 cm core depth) reveal the highest coral content that varies between 30 and 70 surf.%, with overall rather large coral clasts of 1-5 cm in size. Between 270 and 92 cm core depth, the coral content decreases to 30-50 surf.% and also the coral clast sizes decrease to 1-2 cm. For the uppermost part of the core (92 cm to core top), coral content again decreases to 10-30 surf.%. Coral clasts are rather small, with sizes of ~1 cm, only in the uppermost 20 cm, large coral clasts are found.

4.1.2 CT-based classification of cold-water coral preservation patterns of on-mound cores GeoB18127-1 and GeoB18130-1

For the two on-mound cores GeoB18127-1 and GeoB18130-1, the CT analyses allowed for the differentiation of three CPPs following the approach of Titschack et al. (2015). Considering the CWC clast size and orientation, the three CPPs are defined as (i) CPP A: coral framework in living position characterised by large average coral clast size of >-4.7 Φ (>2.6 cm) and variable orientations of up to 90°; (ii) CPP B: slightly collapsed coral framework marked by moderate average coral clast sizes of -4.7 to -4.4 Φ (~2.6-2.1 cm) and orientation < 60°; and (iii) CPP C: coral rubble defined by small average coral clast sizes of <-4.5 Φ (~1.3 cm) and orientations of <45° or no clear orientation (Figs. 2, 3). The average coral content varying between 9 and 23 vol.% could not be applied to clearly distinguish between the CPPs, and the values for clast sizes and orientation of the different CPPs slightly vary between the two cores (see Table S1 in Supplementary Material).

In core GeoB18127-1, CPP A occurs at core depths of 473-395 cm (CPP A_1) and 190-70 cm (CPP A_2; Fig. 2), and CPP B was recognized between CPP A_1 and CPP A_2 at core depths of 360-190 cm. CPP C was identified at various core depths of 563-500 cm (CPP C_1), 500-473 cm (CPP C_2), 395-360 cm (CPP C_3) and 70-0 cm (CPP C_4). It is notable that the CPP C_1, identified at the bottom of the core GeoB18127-1 directly below CPP C_2 exhibits remarkably smaller coral clasts (~2.8 Φ/0.7cm) and lower coral contents (~9 vol.%) compared to all other core sections containing coral rubble (clast size: >-4.2 Φ / >2.1 cm; average coral contents: >16 vol.%; Fig. 2; see also Table S1 in Supplementary Material). In core GeoB18130-1, CPP A was identified at core depths of 106-71 cm, while CPP B occurs below and above CPP A (CPP B_1: 148-106 cm; CPP B_2: 71-34 cm). Coral rubble (CPP C) was only recognised between 34 cm and the core top (Fig. 3).

4.2 Coral ages and coral mound aggradation rates

Four AMS ^{14}C ages were obtained from core MD13-3451G, which range from 13.8 kyr BP to 4.5 kyr BP. One age (13.8 kyr BP) plots into the B/A interstadial, two ages (11.5 kyr BP and 9.5 kyr BP) into the Early Holocene, and one age (4.5 kyr BP) into the Late Holocene (Table 2, Fig. 4). Between 13.8 kyr BP and 11.5 kyr BP, the coral mound AR amounts to 46 cm kyr^{-1}. During the Early Holocene, the coral mound AR was enhanced with 96 cm kyr^{-1} before it dropped to 38 cm kyr^{-1} between 9.5 kyr BP and 4.5 kyr BP (Table 2, Fig. 4).

For core MD13-3452G, eight AMS ^{14}C dates were obtained ranging from 14.0 kyr BP to 3.5 kyr BP (Table 2). Four ages (14.0-12.9 kyr BP) fall into the B/A, three ages (10.9-9.3 kyr BP) into the Early Holocene, and one age (3.5 kyr BP) into the early Late Holocene (Table 2, Fig. 4). During the B/A interstadial, the average coral mound AR amounts to 176 cm kyr^{-1} (min: 132 cm kyr^{-1}, max: 205 cm kyr^{-1}). Between 12.9 kyr BP and 10.9 kyr BP, a low average coral mound AR of 43 cm kyr^{-1} was obtained. In the Early Holocene, the average coral mound AR increased to 107 cm kyr^{-1} (min: 64 cm kyr^{-1}, max: 182 cm kyr^{-1}). The mound AR dropped to 15 cm kyr^{-1} in the following period between 9.3 kyr BP and 3.5 kyr BP (Table 2, Fig. 4).

For the core GeoB18127-1, sixteen U-series ages were obtained, ranging from 14.1 kyr BP to 5.4 kyr BP. Four ages (14.1-13.3 kyr BP) coincide with the B/A interstadial, nine ages (11.1-8.2 kyr BP) with the Early Holocene and four ages (7.8-5.4 kyr BP) with the Mid Holocene (Table 3, Fig. 4). One age at 159 cm core depth (8.55±0.12 kyr BP), is in the error range of the slightly younger age obtained at 189 cm core depth (8.51±0.17 kyr BP; Table 3), and was ignored for the calculation of the coral mound AR. In addition, two ages obtained from *M. oculata* and *L. pertusa* at the same core depth of 79 cm, revealed slightly differing ages of 7.81±0.16 kyr BP and 8.23±0.14 kyr BP, respectively. However, this difference is most likely due to the 3-dimensional complexity of the depositional environment, potentially linked to a reduction of the mound AR (enhanced time averaging effect). The younger age may probably result from the recolonization of *M. oculata*, hence was not used for the calculation of coral mound ARs. During the B/A interstadial, the calculated average mound AR amounts to 113 cm kyr^{-1} (min: 20 cm kyr^{-1}, max: 547 cm kyr^{-1}; Table 3). Between 13.3 kyr BP and 11.1 kyr BP, no CWC ages were obtained, and the coral mound AR during this short interval exhibits low values of 14 cm kyr^{-1}. Between 11.1 kyr BP and 7.6 kyr BP (largely corresponding to the Early Holocene), a mean mound AR of 90 cm kyr^{-1} (min: 40 cm kyr^{-1}, max: 479 cm kyr^{-1}) was obtained. During the Mid Holocene (5.8-5.4 kyr BP; Fig. 4), low coral mound ARs of 21 and 37 cm kyr^{-1} are reported (Table 3; Fig. 4).

Within the core GeoB18130-1, ten U-series ages ranging from 9.4 kyr BP to 5.0 kyr BP were obtained, with seven ages (9.4-7.9 kyr BP) corresponding to the Early Holocene and three ages (7.9-5.0 kyr BP) to the Mid Holocene. One age reversal occurs at the top of the core, most likely due to sediment disturbance during the coring process. The age of 5.28±0.04 kyr BP at 2 cm core depth, was used for the calculation of the coral mound AR. Three ages obtained at the bottom of the core (128-147 cm core depth), show slightly increasing ages from bottom to top (9.37±0.05 kyr BP to 9.40±0.05 kyr BP), though the differences of these ages are within each other's error ranges. This points to a short phase of fast mound formation (9.37-9.40 kyr BP), during which the AR reached values of >270 cm kyr^{-1}. Between 9.1 kyr BP and 7.9 kyr BP (largely corresponding to the Early Holocene), the average coral mound AR was 76 cm kyr^{-1} (min: 24 cm kyr^{-1}, max: 704 cm kyr^{-1}; Table 3, Fig. 4), while between 7.9 kyr BP and 5.0 kyr BP, the coral mound AR declined to ~12 cm kyr^{-1} (Table 3).

4.3 Background palaeo-environmental record from off-mound core GeoB18131-1

4.3.1 Chronology

The chronology of the off-mound core GeoB18131-1 is constrained by six AMS ^{14}C ages, which range between 20.3 kyr BP (at 360 cm core depth) and 0.3 kyr BP (core top; Table 4). The age model is supported by the visual correlation between the $\delta^{18}O_{Cib}$ record and the LR04 $\delta^{18}O$ stack record (Lisiecki and Raymo, 2005). For the tie-point correlation of the lower part of the core (855-360 cm core depth), six visual correlation-points were selected. The obtained age model suggests an age of approximately 110 kyr BP for the bottom of the core (~850 cm core depth), hence the entire record covers the last interglacial (Marine Isotope Stage 5, MIS 5), the last glacial (MIS 2-4) and the recent interglacial (MIS 1; Fig. S2 in Supplementary Material). The $\delta^{18}O_{Cib}$ record shows values of 4.0-1.9‰ for the last interglacial, heavy values of 4.3-3.1‰ for the last glacial, and light values of 3.3-1.5‰ for the Holocene. The calculated sedimentation rate displays an increasing trend towards the Holocene. During the MIS 5, the sedimentation rate was less than 5 cm kyr^{-1}, while during most of the last glacial period, it amounts to 6-9 cm kyr^{-1}. Only during the Last Glacial Maximum (LGM), the sedimentation rate significantly increased to 27 cm kyr^{-1}. During the Holocene, the sedimentation rate varied between 8 cm kyr^{-1} and 21 cm kyr^{-1} (Fig. S2 in Supplementary Material).

4.3.2 Palaeo-environmental proxies

The main aim of this research is to relate the temporal occurrence of CWCs and coral mound development to distinct changes in the palaeo-environment. As the herein presented coral ages reach only 14.1 kyr BP back in time, all presented proxy records are restricted to the last 26 kyr to elucidate any changes across the last glacial-interglacial transition (the entire off-mound core proxy records are presented in Fig. S2 in the Supplementary Material).

During the last 26 kyr, the $\delta^{13}C$ values of the mixed benthic foraminifera ($\delta^{13}C_{Cib}$) range from 1.1‰ to 0.3‰ (Fig. 5A). Before ~13.3 kyr BP, the $\delta^{13}C$ values fluctuate between 0.6‰ and 1.1‰. Between 13.3 kyr BP and 7.6 kyr BP, the $\delta^{13}C_{Cib}$ record displays a conspicuous decreasing trend, declining from 1.0‰ to 0.5‰. Since 7.6 kyr BP, the $\delta^{13}C_{Cib}$ values fluctuate between 0.3‰ and 0.6‰ (Fig. 5B).

The mean grain size ranges from ~17 µm to 5 µm during the last 26 kyr (Fig. 5B). Between 26 kyr BP and ~16 kyr BP, the mean grain size is low with values mainly below 8 µm. Since 16 kyr BP, the mean grain size gradually increases, reaching a maximum value of 17 µm at ~12 kyr BP. Since then it shows a decreasing trend, and the mean grain size value remains again below 8 µm for the last 8 kyr (Fig. 5C).

The BFARs vary between 1 and 27 $\times 10^3$ individuals cm^{-2} kyr^{-1} during the last 26 kyr (Fig. 5C). Before ~17 kyr BP, the BFARs are low, only showing peak values of up to 13 $\times 10^3$ individuals cm^{-2} kyr^{-1} during the LGM. Since ~17 kyr BP, the BFARs show a gradually increasing trend until the highest BFARs of up to ~27 $\times 10^3$ individuals cm^{-2} kyr^{-1} at ~10.8 kyr BP. Between 10.8 kyr BP and 7.6 kyr BP, the BFARs rapidly decline to ~8 ×10^3 individuals cm^{-2} kyr^{-1}. Afterwards, the BFARs remain low, with values of below 5 ×10^3 individuals cm^{-2} kyr^{-1} (Fig. 5D).

5. Discussion

Within the Alboran Sea, the two most common framework CWC species, *L. pertusa* and *M. oculata*, have been found on various seamounts and volcanic banks along the continental slope off Spain, on ridges (e.g., Alboran ridge), and on some mud volcanoes in the western Alboran Sea (Lo Iacono et al., 2008; Margreth et al., 2011; Palomino et al., 2011; De Mol et al., 2012; Lo Iacono et al, 2012; Palomino et al., 2015; Wienberg, 2019). Coral mounds are far more seldom and mainly concentrate in the southern Alboran Sea, comprising the mound clusters of the EMCP and the WMCP (Lo Iacono et al., 2014; Hebbeln, 2019; Wienberg, 2019). The discrepancy between the restricted occurrence of coral mounds in contrast to the widespread distribution of CWCs, though today mainly occurring as fossil accumulations rather than as living occurrences, hints to far more constrained (palaeo-)environmental conditions controlling coral mound formation compared to those promoting CWC growth (Wienberg and Titschack, 2017). The proliferation of CWCs, which is steered by various biotic and abiotic factors such as food supply, water masses properties, local hydrodynamic regime (e.g. Roberts et al., 2006; Davies and Guinotte, 2011) is a prerequisite for coral mound formation. Nevertheless, the construction of CWC mounds as complex geological structures is the result of a well-balanced interplay between a sustained growth of CWC, which form coral frameworks with high sediment baffling capacity, and a contemporaneous supply of sediments stabilizing the biogenic construction (e.g., Thierens et al., 2013; Titschack et al., 2015).

Any variations in the temporal development of coral mounds are reflected by varying ARs as well as by changes in the preservation state of the deposited CWC clasts (see Titschack et al., 2015; Titschack et al., 2016). In this context, high vertical mound aggradation is the result of pronounced CWC growth and enhanced sediment supply, thereby current-transported sediments become entrapped within the coral framework. The fast burying of CWC frameworks prevents them from biodegradation and physical fragmentation, and may even allow the deposition of CWC framework in living position (Titschack et al., 2015). In contrast, during times of reduced CWC growth, coral mounds aggradation is slowed down and can eventually stagnate, the latter being documented as unconformities in the sedimentary record. Furthermore, when the dead coral framework (not covered by an organic tissue) remains exposed for a prolonged time on the mound's surface due to lack of substantial sediment cover, degradation and fragmentation of the coral skeletons may occur, eventually resulting in the formation of coral rubble. Thus, mound ARs calculated from coral dates in combination with the CPPs can be used to reconstruct the temporal development of coral mounds in much detail.

5.1 Cold-water coral mound formation in the southern Alboran Sea since the last deglaciation

5.1.1 Re-activation of coral mound formation during the B/A interstadial

While quite some information exists already on the formation of the coral mounds of the EMCP since the last deglaciation (Fink et al., 2013; Stalder et al., 2015), up to this study no information was available about the temporal development of the mounds in the neighbouring WMCP. Considering their present-day average height of 8-35 m above the seafloor and their additional subsurface extension on one hand (Lo Iacono et al., 2014), and the maximum on-mound core recovery of less than 6 m on the other hand (Table 1), this study, can however only decipher the most recent period(s) of mound development.

The oldest ages obtained from the coral mounds of the WMCP range between 14.1 kyr BP and 12.9 kyr BP, and represent a pronounced coral mound formation stage during the B/A interstadial with high ARs of 113-176 cm kyr^{-1} on average (and even maximum ARs of up to 500 cm kyr^{-1}; Tables 2, 3, Fig. 4). The CPP obtained from the core GeoB18127-1 indicate that coral rubble of B/A age (defined as CPP C_2 in Fig. 2) rest on small-sized CWC rubble (defined as CPP C_1 in Fig. 2). Both CWC rubble-dominated sections are separated by a distinct unconformity. The high fragmentation grade of the pre-B/A CWC rubble deposits indicate that these coral clasts rested for a long time exposed on the mound's surface without any coverage (by sediments or living CWCs). Unfortunately, these CWC clasts were too small and showed strong corrosion avoiding their usage for absolute dating. Therefore, without the support of longer dated core records, the timing of coral mound development before the last deglaciation cannot be further constrained.

Nevertheless, the re-initiation of coral mound formation during the last deglaciation started at ~14.1 kyr BP, interestingly fitting with similar observations obtained from various coral mound records of the EMCP (~13.3-13 kyr BP; Fink et al., 2013; Stalder et al., 2015). The slight temporal off-set (~800 years) in the timing of the deglacial coral re-colonization, and hence, re-initiation in mound formation between both provinces might simply be explained by the limited length of the mound core records available for the EMCP, avoiding to collect coral fragments of early B/A-age. The CPP displayed in core GeoB18127-1, with CWC rubble (CPP C_2) being present at the base of the B/A period along with the associated initial low AR of 21 cm kyr^{-1} (Figs. 2, 4), point to a rather slow post-glacial start-up phase in coral mound formation for the WMCP. This observation contrasts with results from the EMCP, which suggest a sudden and fast start-up phase of CWC colonization (Fink et al., 2013; Titschack et al., 2016). Since ~13.5 kyr BP, the CPP in core GeoB18127-1 changed from CWC rubble to CWC framework being preserved in living position (CPP A_1; Fig. 2), which indicates enhanced CWC growth as well as increased sediment deposition. Also both MD cores show rather large coral clasts (3-5 cm in size) in their lower core intervals that correspond to the B/A (see Fig. S1 in the Supplementary Material), indicating that coral frameworks were rapidly buried by sediments, preventing them from being strongly fragmented. This is further supported by a significant increase of the coral mound ARs to average values of 176-493 cm kyr^{-1} (calculated for cores MD13-3452G and GeoB18127-1; Tables 2, 3, Fig. 4), which are in the range of coeval average ARs of 385-416 cm kyr^{-1} obtained from mounds in the EMCP (Fink et al., 2013; Stalder et al., 2015).

5.1.2 Temporal stagnation in mound formation during the YD cold event

During the YD, coral mound formation significantly slowed down. No coral ages were obtained between 12.9 kyr BP and 11.5 kyr BP, and coral mound ARs significantly decreased to 14-43 cm kyr^{-1} (calculated for cores MD13-3452G and GeoB18127-1; Tables 2,3, Fig. 4). Moreover, a distinct unconformity was identified in core GeoB18127-1 marked by an abrupt change in the CPPs from CWC framework preserved in living position (CPP A_1) to CWC rubble (CPP C_3; Fig. 2). Also for the coral mounds of the EMCP, a distinct reduction in mound aggradation was indicated during the YD (AR: 31-38 cm kyr^{-1}; see also Fig. 5; Fink et al., 2013; Stalder et al., 2015), although based on the available datings it appears that this reduction seems to encompass a shorter time period only corresponding to the late YD (12.2-11.6 kyr BP; Stalder et al., 2015).

5.1.3 Coral mound formation during the Early Holocene

The most recent period of coral mound formation in the WMCP started at ~11.5 kyr BP during the onset of the Early Holocene, and simultaneously to the start of the Early Holocene mound formation period indicated for the EMCP (11.6-11.4 kyr BP; see Fig. 5; Fink et al., 2013; Stalder et al., 2015). As already identified for the B/A mound formation period, there seems to be again a slow start-up phase in mound formation in the WMCP. The CPP in core GeoB18127-1 reveals at the beginning of this period the deposition of CWC rubble (CPP C_3; Fig. 2), and also for the cores MD13-3451G and MD13-3452G, the lower Early Holocene deposits are marked by small sized coral clasts (see Fig. S1 in Supplementary Material). This overall points to hampered CWC growth and low sediment deposition, which is further evidenced by rather low to moderate ARs of 46-97 cm kyr^{-1}. However, already within a few hundreds of years, ARs increased to values of >100 cm kyr^{-1} (even temporarily reaching values of up to 700 cm kyr^{-1}; Tables 2, 3, Fig. 4), although the available CWC ages do not allow to temporally constrain this transition. The increased ARs are accompanied by CPPs that vary between slightly collapsed CWC framework and CWC framework preserved in living position (indicated for cores GeoB18127-1 and GeoB18130-1; Figs. 2, 3). Overall, the average coral mound ARs during the Early Holocene range between 75 and 107 cm kyr^{-1} (Tables 2, 3, Fig. 4). Hence, in comparison to average ARs obtained for the EMCP, which varied between 140 and 291 cm kyr^{-1} (Fink et al., 2013; Stalder et al., 2015), coral mound formation in the WMCP seems to be less pronounced. In addition, while the highest mound aggradation in the EMCP (ARs mainly above 190 cm kyr^{-1}) already occurred directly at the beginning of the Early Holocene mound formation period at 11.6 kyr BP and lasted until ~10.2 kyr BP, the coral mounds of the WMCP experienced their most pronounced Holocene aggradation (ARs mainly above 150 cm kyr^{-1}) between ~9.9 and 8.3 kyr BP, thus about 1700 years later than the boost of the EMCP mound formation (Fig. 5).

5.1.4 Slow-down in coral mound formation since the Mid Holocene

Coral mound formation in the WMCP significantly slowed down since the early Mid Holocene (at ~7.6 kyr BP), which is mainly reflected by a strong decrease of the coral mounds ARs to values of 12-38 cm kyr^{-1} (indicated for all cores; Tables 2, 3, Fig. 4). Moreover, in both GeoB cores, the CPPs abruptly changed from coral framework to CWC rubble (Geob18127-1: CPP A_2 to C_4, Fig. 2; GeoB18130-1: CPP B_2 to C, Fig. 3) during this period, as also shown in both MD cores, where only a sparse occurrence of small-sized coral clasts was indicated, pointing to a reduced CWC growth and a low sediment input, both favouring the fragmentation of coral clasts. For the EMCP, a slow-down in mound formation with a significant decrease of the ARs to 4-22 cm kyr^{-1} already started at ~9.8 kyr BP (Fink et al., 2013; Stalder et al., 2015), thus over 2,000 years earlier compared to the WMCP.

The youngest CWC ages (n=5) obtained for the coral mounds of the WMCP range between 5.8 and 3.5 kyr BP (Tables 2, 3, Fig. 4), hence coral mound formation likely stagnated since the Late Holocene. Present day conditions suggest that CWCs seem to be completely absent from the coral mounds of the WMCP, with some of the ground-truthed mounds being buried by coral-barren sediments (Hebbeln et al., 2015; Lo Iacono et al., 2014). Also for the EMCP, the youngest obtained CWC ages (~2.9-2.6 kyr BP) are of Late Holocene ages, but in contrast to the WMCP, these mounds actually are covered by dead coral framework/rubble with sparse living CWC colonies (Hebbeln et al., 2009; Fink et al., 2013).

5.2 Palaeo-environmental controls on coral mound formation in the southern Alboran Sea

The temporal pattern in mound formation obtained for the coral mounds of the WMCP since the last deglaciation correlates well with distinct changes in the local palaeo-environmental conditions. In particular variations in the surface productivity and food supply, the water column structure, and the near-bottom hydrodynamics were identified to be the most important local or regional driver on the development of the CWC mounds (Fig. 5). Nevertheless, the reactivation of mound formation during the B/A interstadial, both in the WMCP and the EMCP, coincide with a major re-organisation of the thermohaline circulation in the entire Mediterranean basin. The rapid last deglacial sea-level rise (Fig. 5; Lambeck et al., 2014) resulted in an increased injection of low saline Atlantic waters due to a deepening of the Gibraltar sill (Sierro et al., 2005). Moreover, the enhanced glacial melting in the Alps and Apennines increased the inflow of freshwater into the Mediterranean Basin (e.g., Cacho et al., 2002; Ivy-Ochs et al., 2007; Rogerson et al., 2008), both leading to a freshening and reduced density of the surface waters. Concurrently, the sea surface temperatures increased up to 14°C (e.g., Balearic Sea; Dubois-Dauphin et al., 2017). All these processes resulted in a slowdown of the Mediterranean Sea thermohaline circulation and caused a collapse of deep-water (WMDW) production in the western Mediterranean Sea (Gulf of Lion), which led to an increased stratification of the water column and weakened ventilation of intermediate and deep-water masses (Cacho et al., 2001; Sierro et al., 2005; Rogerson et al., 2008; Toucanne et al., 2012). At the same time, the production of LIW in the eastern Mediterranean Sea (Levantine Basin) was enhanced, which caused intensification and increased inflow of the LIW into the western basin (Jiménez-Espejo et al., 2015). The strong influence of the LIW at the intermediate depths in the Alboran Sea since the last deglaciation is also documented in the neodymium isotopic composition of CWCs collected from the EMCP, though the Alboran Sea seems to be rather insensitive to hydrological variations of the LIW, at least since 13.5 kyr BP until present (Dubois-Dauphin et al., 2017).

Studies from various sites in the western Mediterranean Sea revealed that the surface productivity gradually increased during the B/A (Fig. 5) due to a shoaling of the nutricline, and consequently also the export of organic matter was enhanced (Cacho et al., 2002; Jimenez-Espejo et al., 2008; Rogerson et al., 2008; Ausín et al., 2015; Jimenez-Espejo et al., 2015) resulting in the deposition of the organic rich layer 1 (ORL1; 14.5-8.2 kyr BP) in the deep western Mediterranean Sea (Cacho et al., 2002). The BFAR record from the WMCP reveals a low export production during the last glacial before it significantly increased since 14 kyr BP, reached its maximum during the Early Holocene and dropped rapidly at the onset of the Mid Holocene (Fig. 6). This suggests a more or less synchronous increase of the BFAR export production with the formation of the ORL1, supporting the enhanced surface productivity, and even more important, highlighting an improved food delivery to the WMCP during this time interval since the deglaciation until the Mid Holocene has likely favoured the proliferation of CWCs and mound formation within the region, by contributing to their food supply (Fig. 5).

However, considerable differences in the BFAR between the two main mound formation phases marked by similar mound aggradation rates call for additional parameters in addition to palaeo-productivity that control mound formation. Interestingly, the grain-size distribution shows a similar pattern as the BFAR with coarser sediments occurring between 15 and 8 kyr BP (Fig. 5). The enhanced hydrodynamic energy reflected by this coarsening of the sediments further contributed to the food supply of the CWCs. The change in the grain size distribution coincides with our $\delta^{13}C_{Cib}$ record, which here is adopted to trace past changes in the water column structure (Fig. 5). During the last glacial, the intermediate depths of the WMCP were influenced by waters with relatively high $\delta^{13}C_{Cib}$ values (0.8-1.1‰; Fig. 5), which we interpret to represent the effect of a dominant influence of the MAW coinciding with the sea level considerably lower than today. On the contrary after the cessation of deglacial sea-level rise and the final establishment of the modern circulation, the intermediate depths of the WMCP were mainly bathed by waters with relatively low $\delta^{13}C_{Cib}$ values (0.3-0.6‰; Fig. 5), which are likely due to the predominance of the LIW. However, from the B/A interstadial to the Mid Holocene (~13.3-7.6 kyr BP), the $\delta^{13}C_{Cib}$ record shows a gradual change from MAW to LIW dominance, though also revealing strong fluctuations (Fig. 5). Thus, we assume that in pace with the deglacial sea level rise, the coral mounds of the WMCP, which today occur at water depths of 300-490 m (Lo Iacono et al., 2014), were bathed by the MAW before the B/A interstadial. Between the B/A interstadial and Early Holocene the mounds became affected by the interface between the MAW and the LIW, and were mainly influenced by the LIW since the Mid Holocene, when the water mass interface was shifted towards shallower depths above the coral mounds (Fig. 6). Interestingly, the time interval when the coral mounds of the WMCP were placed within the interface between the MAW and the LIW – marked by the strong gradient in the $\delta^{13}C_{cib}$ record - almost exactly encompasses the timing of mound formation in the WMCP during the B/A interstadial (14.1-12.9 kyr BP) and the Early Holocene (11.6-7.6 kyr BP; Figs. 4, 5).

Common features that occur at the interface between two water masses of different densities are internal waves (Small and Martin, 2002; Pomar et al., 2012;). Such waves propagate along the pycnocline, due to friction between the two water bodies caused by different flow velocities, and eventually break against facing slopes (Pomar et al., 2012). Therefore, internal waves are a potentially relevant source of turbulent energy as they enable mixing and particle re-suspension, and hence the lateral transportation of particulate organic materials. Moreover, these features can force the accumulation of particulate material, and hence, the formation of nepheloid layers (Mienis et al., 2007). The positive feedback of internal waves on mound formation is described for various modern coral mound settings in the NE Atlantic (Frederiksen et al., 1992; White et al., 2005; Mienis et al., 2007; Davies et al., 2009; White and Dorschel, 2010; Hebbeln et al., 2014). Internal waves transport fresh or re-suspend recently deposited food particles with increased velocity to the CWCs thriving on mounds (Mienis et al., 2007). Thereby, they act as a nutritional pump that makes food particles repeatedly available for CWCs, flushing particles laterally through the CWC framework, thus enhancing the chance for the coral polyps to catch them (Davies et al., 2009; Mienis et al., 2009; Hebbeln et al., 2016). Also for the fossil record, a strong relationship between the existence of a water mass interface and coral mound formation has already been postulated. For example, mound aggradation along the Irish margin (Porcupine Seabight) was active when the interface between the Mediterranean Outflow Water and the Eastern North Atlantic Water was placed towards the depth level of the mounds, thereby the stable water mass stratification between both water masses caused enhanced food supply (Raddatz et al., 2014). Recently, the positive effect of internal waves has been hypothesised for a coral mound province in the Gulf of Mexico (Campeche Bank; Matos et al., 2017). There, mound formation is restricted to interglacial periods, when internal waves propagated along the pycnocline between the Atlantic Intermediate Water and the Tropical Atlantic Central Water, while during glacial times this water mass interface was shifted away from the coral mounds (Matos et al., 2017). It is very likely that such a scenario is also valid for the WMCP, where internal waves propagating along the MAW-LIW-interface enhanced the supply of food particles to the CWCs and hence promoted the pronounced aggradation of the mounds during the B/A and Early Holocene (Fig. 6). The enhanced hydrodynamic energy resulting from the internal waves along the water mass interface is reflected by the grain size data from the off-mound record in the WMCP and the EMCP (Figs. 5, 6).

By comparing the palaeo-environmental conditions between the WMCP and the neighbouring EMCP, very similar trends with respect to export production and near-bottom hydrodynamics are indicated for the past 23 kyr (Fig. 5; see also Fink et al., 2013). However, the mounds of the EMCP experienced a slightly earlier (at ~9.8 kyr BP) slow-down in mound formation during the Early Holocene (Fink et al., 2013; Stalder et al., 2015) compared to the mounds of the WMCP (at ~7.6 kyr BP; Fig. 5). This might simply reflect the natural mound formation variability along continental margins as was recently shown by Wienberg et al. (2018). These authors identified distinct temporal differences in mound formation stages within a giant coral mound province off Mauritania, even for directly neighbouring coral mounds. Alternatively, the temporal offset in mound formation between the EMCP and the WMCP might be related to the influence of the Cape Tres Forcas, which today separates both provinces and whose morphology probably significantly modified the circulation pattern in pace with the rising sea level since the last deglaciation. During the LGM, the sea level was ~130 m lower than at present (Fig. 5), and the Moroccan coastline was located much further off-shore, thus much closer to the coral mounds of the WMCP and the EMCP (see also Lo Iacono et al., 2014). At ~14.5 kyr BP the sea-level rapidly rose about 20 m in about 500 years (Deschamps et al., 2012), and reached the present-day level between 8 and 6 kyr BP (Lambeck and Chappell, 2001; Lambeck et al., 2014; Fig. 5). As suggested by Lo Iacono et al. (2014), the morphological alteration of the Cape Tres Forcas due to the sea-level rise probably modified the current regime and subsequent sedimentation rates in the WMCP, leading to the demise of coral mounds.

One period that remains enigmatic is the YD cold event, when mound formation temporarily stagnated, though our off-mound record reveals significant enhancement of productivity and hydrodynamics (Figs. 5, 6). Enhanced productivity conditions in combination with a well-ventilated, high energetic intermediate water mass regime during the YD was also assumed for other sites in the western Mediterranean Sea (Bárcena et al., 2001; Rogerson et al., 2008; McCulloch et al., 2010; Margreth et al., 2011; Toucanne et al., 2012). However, while these overall optimal environmental conditions explain the frequent reports of corals of YD-age from various sites in the Mediterranean Sea (Balearic, Tyrrhenian, Ionian and Aegean Seas; McCulloch et al., 2010; Taviani et al., 2011; Fink et al., 2015), the reduced occurrence (or even absence) of CWCs in the southern Alboran Sea point to rather local environmental controls that suppressed their proliferation. Fink et al. (2015) assumed that this local control on CWC growth in the southern Alboran Sea might be related to changes in the two-gyres-system that induced upwelling and density fronts in the upper 200-300 m (Heburn and La Violette, 1990).

6. Conclusions

Within the Alboran Sea, coral mounds formed by the scleractinian framework-forming CWCs *L. pertusa* and *M. oculata* were so far only discovered along its southern margin just 15-30 km off the Moroccan coastline. These mounds are grouped in two provinces, the WMCP and EMCP, which are located east and west of the Spanish enclave Melilla (Cape Tres Forcas) in intermediate water depths of 200-450 m

(Lo Iacono et al., 2014; Hebbeln, 2019). This study provided for the first time insight into the temporal evolution of the coral mounds in the WMCP and clearly revealed that mound formation re-initiated (almost) simultaneously in both provinces with the onset of the last deglaciation. Subsequently, the mounds experienced periods of pronounced aggradation corresponding to the B/A interstadial and the Early Holocene. Highest ARs were reached during the B/A, with average ARs of 1-2 m kyr^{-1} obtained for the WMCP. These ARs are in the range of or even above the values found for mound provinces in the NE Atlantic (e.g., Frank et al., 2009; Wienberg and Titschack, 2017). The CPPs identified for the mounds of the WMCP indicate for both periods a slow start-up phase rapidly followed by a "booster" stage in mound formation which partly supports an early mound evolution model introduced by Henriet et al. (2002).

The re-initiation of mound formation and subsequent mound development in the southern Alboran Sea was likely the result of (i) the strong hydrodynamics triggered by internal waves related to the sea level-driven re-organisation of the water column structure, and (ii) the concurrently enhanced ocean productivity. For modern Atlantic coral mound settings, internal waves are frequently observed to develop along pycnoclines related to water mass boundaries. They create enhanced turbulent energy and lateral transport (and/or enrichment) of particulate material (food, sediments; e.g., Mienis et al., 2007; White et al., 2005), thus supporting CWC growth as well as mound formation. We assume that such a scenario also promoted mound formation in the southern Alboran Sea from the last deglaciation until the end of the Early Holocene (see also Fink et al., 2013). During the Mid Holocene, the MAW-LIW-interface shifted to shallower water depths above the mounds and altered the environmental conditions at the sea floor to a less turbulent condition. At the same time, the area turned into an oligotrophic setting. These caused a significant slow-down (EMCP) and even stagnation (WMCP) in mound formation that persists until today.

The water column structure most likely played a dominant role in controlling mound formation in the southern Alboran Sea. However, the locally and temporarily restricted processes might also have influenced the development of the coral mounds. During the YD, mound formation was suppressed in both provinces which might be related to the changes of the two gyre circulation that triggering upwelling and density fronts at intermediate water depths (Fink et al., 2015; Heburn and La Violette, 1990). Moreover, slight temporal offsets in mound formation identified between the two provinces might be related to the Cape Tres Forcas that acts as a morphological barrier possibly affecting the hydrodynamic processes in both provinces in a different manner. However, these offsets also simply might reflect the natural variability in mound formation, which according to recent studies seems to be a common pattern (even between directly neighboring coral mounds) rather than an exceptional feature (e.g., Wienberg et al., 2018).

While this study provides detailed insight into the most recent coral mound development in the southern Alboran Sea, the timing and environmental controls of mound formation before the last deglaciation remains unknown. Only with the recovery of longer sedimentary records, we may possibly elucidate any large-scale pattern related to older climate fluctuations, as identified for NE Atlantic mound provinces (e.g., Frank et al., 2011).

Acknowledgements

We like to thank the nautical and scientific crews for on-board assistance during RV Marion Dufresne cruise MD194 "Gateways" and during RV Maria S. Merian cruise MSM36 "MoccoMeBo". We wish to acknowledge EC FP7 EuroFleets Project for granting the MD194 cruise and related logistics under project grant No. 228344, the *Deutsche Forschungsgemeinschaft* (DFG) for providing ship time to realize cruise MSM36 and the EC Marie Curie single action "Geo-Habit" (GA29874) for supporting the absolute dating of the MD cores presented in this study. Cruise MSM36 was further supported through the DFG Research Center/Cluster of Excellence "MARUM – The Ocean in the Earth System". This study received funding from the DFG-project "MoccAMeBo" (HE 3412/18-1). The scholarship of H. Wang is funded by the Chinese Scholar Council. We thank the GeoB Core Repository at the MARUM (Center for Marine Environmental Sciences, University of Bremen, Germany) for the assistance in providing GeoB sediment cores and sample material. This research used data acquired at the XRF Core Scanner Lab at the MARUM. Klinikum Bremen-Mitte (Bremen, Germany) is gratefully acknowledged for providing their facilities for the performed computed tomographies (CT), in particular A.-J. Lemke, H. Liebe and C. Timann are thanked for performing the CT scans and their support during the measurements. D. Reyes Macaya, G. Martínez-Méndez and G. Schmiedl are thanked for their support in the identification of benthic foraminifera and the interpretation of the $\delta^{13}C$ data. M. Bartels is thanked for his support in the benthic foraminifera counting. We further acknowledge H. Kuhnert, B. Meyer-Schack and V. Lukies (MARUM) for lab support during stable isotope and XRF measurements, and A. Schröder-Ritzrau and R. Eichstädter (IUP, University of Heidelberg, Germany) for support during Uranium-series dating of cold-water corals. The Poznan Radiocarbon Laboratory (Poznan, Poland) is thanked for AMS ^{14}C dating of the cold-water corals and the mixed planktonic foraminifera samples.

References

Ausín, B., Flores, J.A., Sierro, F.J., Bárcena, M.A., Hernández-Almeida, I., Francés, G., Gutiérrez-Arnillas, E., Martrat, B., Grimalt, J.O., Cacho, I., 2015. Coccolithophore productivity and surface water dynamics in the Alboran Sea during the last 25kyr. Palaeogeography, Palaeoclimatology, Palaeoecology 418, 126-140.

Baldacci, A., Corsini, G., Grasso, R., Manzella, G., Allen, J.T., Cipollini, P., Guymer, T.H., Snaith, H.M., 2001. A study of the Alboran sea mesoscale system by means of empirical orthogonal function decomposition of satellite data. Journal of Marine Systems 29, 293-311.

Bárcena, M.A., Cacho, I., Abrantes, F., Sierro, F.J., Grimalt, J.O., Flores, J.A., 2001. Paleoproductivity variations related to climatic conditions in the Alboran Sea (western Mediterranean) during the last glacial–interglacial transition: the diatom record. Palaeogeography, Palaeoclimatology, Palaeoecology 167, 337-357.

Berger, W., Herguera, J., 1992. Reading the sedimentary record of the ocean’s productivity, in: Falkowski, P.G., Woodhead, A.D., Vivirito, K. (Eds.), Primary productivity and biogeochemical cycles in the sea. Springer US, Boston, MA, pp. 455-486.Brankart, J.-M., Pinardi, N., 2001. Abrupt cooling of the Mediterranean Levantine Intermediate Water at the beginning of the 1980s: Observational evidence and model simulation. Journal of Physical Oceanography 31, 2307-2320.

Büscher, J.V., Form, A.U., Riebesell, U., 2017. Interactive effects of ocean acidification and warming on growth, fitness and survival of the cold-water coral *Lophelia pertusa* under different food availabilities. Frontiers in Marine Science 4.

Cacho, I., Grimalt, J.O., Canals, M., 2002. Response of the Western Mediterranean Sea to rapid climatic variability during the last 50,000 years: a molecular biomarker approach. Journal of Marine Systems 33-34, 253-272.

Cacho, I., Grimalt, J.O., Canals, M., Sbaffi, L., Shackleton, N.J., Schönfeld, J., Zahn, R., 2001. Variability of the western Mediterranean Sea surface temperature during the last 25,000 years and its connection with the Northern Hemisphere climatic changes. Paleoceanography 16, 40-52.

Cheng, H., Adkins, J., Edwards, R.L., Boyle, E.A., 2000. U-Th dating of deep-sea corals. Geochimica et Cosmochimica Acta 64, 2401-2416.

Collart, T., Verreydt, W., Hernández-Molina, F.J., Llave, E., León, R., Gómez-Ballesteros, M., Pons-Branchu, E., Stewart, H., Van Rooij, D., 2018. Sedimentary processes and cold-water coral mini-mounds at the Ferrol canyon head, NW Iberian margin. Progress in Oceanography.

Comas, M., Pinheiro, L., Ivanov, M., TTR-17 Leg 1 Scientific Party, 2009. Geo-Marine Research on the Mediterranean and European-Atlantic Margins. International Conference and TTR-17 Post-Cruise Meeting of the Training-through-Research Programme. Granada, Spain, 2-5 February 2009, in: Comas, M., Suzyumov, A. (Eds.), Deep-water coral mounds in the Alboran Sea: the Melilla mound field revisited. IOC Workshop Report, NO. 220 (English), UNESCO, 2009, p. 52.

Correa, T.B.S., Eberli, G.P., Grasmueck, M., Reed, J.K., Correa, A.M.S., 2012. Genesis and morphology of cold-water coral ridges in a unidirectional current regime. Marine Geology 326-328, 14-27.

Curry, W.B., Duplessy, J.C., Labeyrie, L., J. Shackleton, N., 1988. Changes in the distribution of $\delta^{13}C$ of deep water ΣCO_2 between the Last Glaciation and the Holocene.

Curry, W.B., Oppo, D.W., 2005. Glacial water mass geometry and the distribution of $\delta^{13}C$ of ΣCO_2 in the western Atlantic Ocean. Paleoceanography 20, PA1017.

D'Ortenzio, F., Ribera d'Alcalà , M., 2009. On the trophic regimes of the Mediterranean Sea: a satellite analysis. Biogeosciences 6, 139-148.

Davies, A.J., Duineveld, G.C., Lavaleye, M.S., Bergman, M.J., van Haren, H., Roberts, J.M., 2009. Downwelling and deep-water bottom currents as food supply mechanisms to the cold-water coral *Lophelia pertusa* (Scleractinia) at the Mingulay Reef Complex. Limnology and Oceanography 54, 620-629.

Davies, A.J., Guinotte, J.M., 2011. Global habitat suitability for framework-forming cold-water corals. PLoS ONE 6, e18483.

Davies, A.J., Wisshak, M., Orr, J.C., Murray Roberts, J., 2008. Predicting suitable habitat for the cold-water coral *Lophelia pertusa* (Scleractinia). Deep Sea Research Part I: Oceanographic Research Papers 55, 1048-1062.

De Haas, H., Mienis, F., Frank, N, Richter, T.O., Steinbacher, R., de Stigter, H., van der Land, C., van Weering, T.C.E., 2009. Morphology and sedimentology of (clustered) cold-water coral mounds at the south Rockall Trough margins, NE Atlantic Ocean. Facies 55, 1-26.

De Mol, B., Amblas, D., Calafat, A., Canals, M., Duran, R., Lavoie, C., Muñoz, A., Rivera, J., 2012. 60 - Cold-Water Coral Colonization of Alboran Sea Knolls, Western Mediterranean Sea A2 - Harris, Peter T, in: Baker, E.K. (Ed.), Seafloor Geomorphology as Benthic Habitat. Elsevier, London, pp. 819-829.

De Mol, B., Van Rensbergen, P., Pillen, S., Van Herreweghe, K., Van Rooij, D., McDonnell, A., Huvenne, V., Ivanov, M., Swennen, R., Henriet, J.-P., 2002. Large deep-water coral banks in the Porcupine Basin, southwest of Ireland. Marine Geology 188, 193-231.

Deschamps, P., Durand, N., Bard, E., Hamelin, B., Camoin, G., Thomas, A.L., Henderson, G.M., Okuno, J.i., Yokoyama, Y., 2012. Ice-sheet collapse and sea-level rise at the Bølling warming 14,600 years ago. Nature 483, 559.

Dorschel, B., Hebbeln, D., Ruggeberg, A., Dullo, W., Freiwald, A., 2005. Growth and erosion of a cold-water coral covered carbonate mound in the Northeast Atlantic during the Late Pleistocene and Holocene. Earth and Planetary Science Letters 233, 33-44.

Dubois-Dauphin, Q., Montagna, P., Siani, G., Douville, E., Wienberg, C., Hebbeln, D., Liu, Z., Kallel, N., Dapoigny, A., Revel, M., Pons-Branchu, E., Taviani, M., Colin, C., 2017. Hydrological variations of the intermediate water masses of the western Mediterranean Sea during the past 20 ka inferred from neodymium isotopic composition in foraminifera and cold-water corals. Climate of the Past 13, 17-37.

Duineveld, G.C., Lavaleye, M.S., Bergman, M.J., De Stigter, H., Mienis, F., 2007. Trophic structure of a cold-water coral mound community (Rockall Bank, NE Atlantic) in relation to the near-bottom particle supply and current regime. Bulletin of Marine Science 81, 449-467.

Duineveld, G.C.A., Jeffreys, R.M., Lavaleye, M.S.S., Davies, A.J., Bergman, M.J.N., Watmough, T., Witbaard, R., 2012. Spatial and tidal variation in food supply to shallow cold-water coral reefs of the Mingulay Reef complex (Outer Hebrides, Scotland). Marine Ecology Progress Series 444, 97-115.

Dullo, W.-C., Flögel, S., Rüggeberg, A., 2008. Cold-water coral growth in relation to the hydrography of the Celtic and Nordic European continental margin. Marine Ecology Progress Series 371, 165-176.

Ehrmann, W.U., Thiede, J., 1985. History of mesozoic and cenozoic sediment fluxes to the-North Atlantic Ocean, Contributions to Sedimentology E. Schweizerbart, Stuttgart, pp. 105-109.

Eisele, M., Frank, N., Wienberg, C., Hebbeln, D., López Correa, M., Douville, E., Freiwald, A., 2011. Productivity controlled cold-water coral growth periods during the last glacial off Mauritania. Marine Geology 280, 143-149.

Fabres, J., Calafat, A., Sanchez-Vidal, A., Canals, M., Heussner, S., 2002. Composition and spatio-temporal variability of particle fluxes in the Western Alboran Gyre, Mediterranean Sea. Journal of Marine Systems 33, 431-456.

Fink, H.G., Wienberg, C., De Pol-Holz, R., Hebbeln, D., 2015. Spatio-temporal distribution patterns of Mediterranean cold-water corals (*Lophelia pertusa* and *Madrepora oculata*) during the past 14,000 years. Deep Sea Research Part I: Oceanographic Research Papers 103, 37-48.

Fink, H.G., Wienberg, C., De Pol-Holz, R., Wintersteller, P., Hebbeln, D., 2013. Cold-water coral growth in the Alboran Sea related to high productivity during the Late Pleistocene and Holocene. Marine Geology 339, 71-82.

Flögel, S., Dullo, W.C., Pfannkuche, O., Kiriakoulakis, K., Rüggeberg, A., 2014. Geochemical and physical constraints for the occurrence of living cold-water corals. Deep Sea Research Part II 99, 19-26.

Fosså, J.H., Lindberg, B., Christensen, O., Svellingen, I., Mortensen, P.B., Alsvag, J., 2005. Mapping of Lophelia reefs in Norway: experiences and survey methods. In: Freiwald A, Roberts JM (eds) Cold-Water Corals and Ecosystems. Springer, Berlin, pp. 359-391.

Frank, N., Freiwald, A., Correa, M.L., Wienberg, C., Eisele, M., Hebbeln, D., Van Rooij, D., Henriet, J.-P., Colin, C., van Weering, T., 2009. Northeastern Atlantic cold-water coral reefs and climate. Geology 39, 743-746.

Frank, N., Freiwald, A., Correa, M.L., Wienberg, C., Eisele, M., Hebbeln, D., Van Rooij, D., Henriet, J.P., Colin, C., van Weering, T., de Haas, H., Buhl-Mortensen, P., Roberts, J.M., De Mol, B., Douville, E., Blamart, D., Hatte, C., 2011. Northeastern Atlantic cold-water coral reefs and climate. Geology 39, 743-746.

Frank, N., Paterne, M., Ayliffe, L., van Weering, T., Henriet, J.-P., Blamart, D., 2004. Eastern North Atlantic deep-sea corals: tracing upper intermediate water $\Delta^{14}C$ during the Holocene. Earth and Planetary Science Letters 219, 297-309.

Frederiksen, R., Jensen, A., Westerberg, H., 1992. The distribution of the scleractinian coral *Lophelia pertusa* around the Faroe islands and the relation to internal tidal mixing. Sarsia 77, 157-171.

Freiwald, A., 2002. Reef-forming cold-water corals, in: Wefer, G., Billett, D., Hebbeln, D., Jorgensen, B.B., Schlüter, M., van Weering, T.C.E. (Eds.), Ocean Margin Systems. Springer, Berlin, Heidelberg, pp. 365-385.

Glogowski, S., Dullo, W.-C., Feldens, P., Liebetrau, V., von Reumont, J., Hühnerbach, V., Krastel, S., Wynn, R.B., Flögel, S., 2015. The Eugen Seibold coral mounds offshore western Morocco: oceanographic and bathymetric boundary conditions of a newly discovered cold-water coral province. Geo-Marine Letters 35, 257-269.

Hebbeln, D., 2019. Highly variable submarine landscapes in the Alborán Sea created by cold-water corals. In: Orejas C, Jiménez C, Mediterranean Cold-Water Corals: Past, Present and Future, Springer series: Coral Reefs of the World.

Hebbeln, D., Bender, M., Gaide, S., Titschack, J., Vandorpe, T., Van Rooij, D., Wintersteller, P., Wienberg, C., 2019. Thousands of cold-water coral mounds along the Moroccan Atlantic continental margin: distribution and morphometry. Marine Geology in press.

Hebbeln, D., Van Rooij, D., Wienberg, C., 2016. Good neighbours shaped by vigorous currents: Cold-water coral mounds and contourites in the North Atlantic. Marine Geology 378, 171-185.

Hebbeln, D., Wienberg, C., Bartels, M., Bergenthal, M., Fraink, N., Henriet, J.-P., Kaszemeik, K., Klar, S., Klein, T., Krengel, T., Kuhnert, M., Meyer-Schack, B., Noorlander, C., Reuter, M., Rosiak, U., Schmidt, W., Seeba, H., Seiter, C., Stange, N., Terhzaz, L., Van Rooij, D., cruise participants, 2015. MoccoMeBo Climate-driven development of Moroccan cold-water coral mounds revealed by MeBo-drilling: Atlantic vs. Mediterranean settings - Cruise MSM36 - February 18 - March 17, 2014 - Malaga (Spain) - Las Palmas (Spain). MARIA S. MERIAN-Berichte, MSM36, 47 pp., DFG-Senatskommission für Ozeanographie.

Hebbeln, D., Wienberg, C., Beuck, L., Freiwald, A., Wintersteller, P., cruise participants, 2009. Report and preliminary results of RV POSEIDON Cruise POS 385 “Cold-Water Corals of the Alboran Sea (western Mediterranean Sea)”, Faro–Toulon, May 29–June 16, 2009, Reports of the Department of Geosciences (GeoB), University of Bremen, No. 273, p. 79.

Hebbeln, D., Wienberg, C., Wintersteller, P., Freiwald, A., Becker, M., Beuck, L., Dullo, C., Eberli, G.P., Glogowski, S., Matos, L., Forster, N., Reyes-Bonilla, H., Taviani, M., 2014. Environmental forcing of the Campeche cold-water coral province, southern Gulf of Mexico. Biogeosciences 11, 1799-1815.

Heburn, G.W., La Violette, P.E., 1990. Variations in the structure of the anticyclonic gyres found in the Alboran Sea. Journal of Geophysical Research 95, 1599.

Henriet, J.P., Guidard, S., and the ODP "Proposal 573" Team, 2002. Carbonate mounds as a possible example for microbial activity in geological processes, in: Wefer, G., Billett, D., Hebbeln, D., Jorgensen, B.B., Schlüter, M., van Weering, T.C.E. (Eds.), Ocean Margin Systems. Springer, Berlin, Heidelberg, pp. 439-455.

Henry, L.-A., Roberts, J.M., 2007. Biodiversity and ecological composition of macrobenthos on cold-water coral mounds and adjacent off-mound habitat in the bathyal Porcupine Seabight, NE Atlantic. Deep Sea Research Part I: Oceanographic Research Papers 54, 654-672.

Huvenne, V.A.I., Masson, D.G., Wheeler, A.J., 2009. Sediment dynamics of a sandy contourite: the sedimentary context of the Darwin cold-water coral mounds, Northern Rockall Trough. International Journal of Earth Sciences 98, 865-884.

Ivy-Ochs, S., Kerschner, H., Schlüchter, C., 2007. Cosmogenic nuclides and the dating of Lateglacial and Early Holocene glacier variations: The Alpine perspective. Quaternary International 164-165, 53-63.

Jimenez-Espejo, F.J., Martinez-Ruiz, F., Rogerson, M., González-Donoso, J.M., Romero, O.E., Linares, D., Sakamoto, T., Gallego-Torres, D., Rueda Ruiz, J.L., Ortega-Huertas, M., Perez Claros, J.A., 2008. Detrital input, productivity fluctuations, and water mass circulation in the westernmost Mediterranean Sea since the Last Glacial Maximum. Geochemistry, Geophysics, Geosystems 9, Q11U02.

Jiménez-Espejo, F.J., Pardos-Gené, M., Martínez-Ruiz, F., García-Alix, A., van de Flierdt, T., Toyofuku, T., Bahr, A., Kreissig, K., 2015. Geochemical evidence for intermediate water circulation in the westernmost Mediterranean over the last 20kyr BP and its impact on the Mediterranean Outflow. Global and Planetary Change 135, 38-46.

Kano, A., Ferdelman, T.G., Williams, T., Henriet, J.-P., Ishikawa, T., Kawagoe, N., Takashima, C., Kakizaki, Y., Abe, K., Sakai, S., 2007. Age constraints on the origin and growth history of a deep-water coral mound in the northeast Atlantic drilled during Integrated Ocean Drilling Program Expedition 307. Geology 35, 1051-1054.

Lambeck, K., Chappell, J., 2001. Sea Level Change Through the Last Glacial Cycle. Science 292, 679-686.

Lambeck, K., Rouby, H., Purcell, A., Sun, Y., Sambridge, M., 2014. Sea level and global ice volumes from the Last Glacial Maximum to the Holocene. Proceedings of the National Academy of Sciences 111, 15296-15303.

Lisiecki, L.E., Raymo, M.E., 2005. A Pliocene-Pleistocene stack of 57 globally distributed benthic $\delta^{18}O$ records. Paleoceanography 20, PA1003.

Lo Iacono, C., Gràcia, E., Bartolomé, R., Coiras, E., Jose Dañobeitia, J., Acosta, J., 2012. 49 - Habitats of the Chella Bank, Eastern Alboran Sea (Western Mediterranean) A2 - Harris, Peter T, in: Baker, E.K. (Ed.), Seafloor Geomorphology as Benthic Habitat. Elsevier, London, pp. 681-690.

Lo Iacono, C., Gràcia, E., Diez, S., Bozzano, G., Moreno, X., Dañobeitia, J., Alonso, B., 2008. Seafloor characterization and backscatter variability of the Almería Margin (Alboran Sea, SW Mediterranean) based on high-resolution acoustic data. Marine Geology 250, 1-18.

Lo Iacono, C., Gràcia, E., Ranero, C.R., Emelianov, M., Huvenne, V.A.I., Bartolomé, R., Booth-Rea, G., Prades, J., 2014. The West Melilla cold water coral mounds, Eastern Alboran Sea: Morphological characterization and environmental context. Deep Sea Research Part II: Topical Studies in Oceanography 99, 316-326.

Lo Iacono, C., Huvenne CAI, Gonzalez LV, Vertino A, Van Rooij D, Gràcia E, Ranero CR, the GATEWAYS Cruise Party (2016) Living reefs and CWC mounds in the Alboran Sea (Western Mediterranean). Holocene evolution and present-day conditions. In: Abstracts of the 6th International Symposium on Deep-Sea Corals, Boston, 11-16 September 2016.

Lo Iacono, C., Savini, A., Basso, D., 2018. Cold-Water Carbonate Bioconstructions, in: Micallef, A., Krastel, S., Savini, A. (Eds.), Submarine Geomorphology. Springer International Publishing, Cham, pp. 425-455.

Margreth, S., Gennari, G., Rüggeberg, A., Comas, M.C., Pinheiro, L.M., Spezzaferri, S., 2011. Growth and demise of cold-water coral ecosystems on mud volcanoes in the West Alboran Sea: The messages from the planktonic and benthic foraminifera. Marine Geology 282, 26-39.

Martínez-Méndez, G., Hebbeln, D., Mohtadi, M., Lamy, F., De Pol-Holz, R., Reyes-Macaya, D., Freudenthal, T., 2013. Changes in the advection of Antarctic Intermediate Water to the northern Chilean coast during the last 970 kyr. Paleoceanography 28, 607-618.

Matos, L., Mienis, F., Wienberg, C., Frank, N., Kwiatkowski, C., Groeneveld, J., Thil, F., Abrantes, F., Cunha, M.R., Hebbeln, D., 2015. Interglacial occurrence of cold-water corals off Cape Lookout (NW Atlantic): First evidence of the Gulf Stream influence. Deep Sea Research Part I: Oceanographic Research Papers 105, 158-170.

Matos, L., Wienberg, C., Titschack, J., Schmiedl, G., Frank, N., Abrantes, F., Cunha, M.R., Hebbeln, D., 2017. Coral mound development at the Campeche cold-water coral province, southern Gulf of Mexico: Implications of Antarctic Intermediate Water increased influence during interglacials. Marine Geology 392, 53-65.

McCulloch, M., Taviani, M., Montagna, P., López Correa, M., Remia, A., Mortimer, G., 2010. Proliferation and demise of deep-sea corals in the Mediterranean during the Younger Dryas. Earth and Planetary Science Letters 298, 143-152.

McGregor, H.V., Dupont, L., Stuut, J.-B.W., Kuhlmann, H., 2009. Vegetation change, goats, and religion: a 2000-year history of land use in southern Morocco. Quaternary Science Reviews 28, 1434-1448.

Merkus, H.G., 2009. Particle size measurements: fundamentals, practice, quality. Springer Science & Business Media.

Mienis, F., de Stigter, H.C., de Haas, H., van Weering, T.C.E., 2009. Near-bed particle deposition and resuspension in a cold-water coral mound area at the Southwest Rockall Trough margin, NE Atlantic. Deep Sea Research Part I: Oceanographic Research Papers 56, 1026-1038.

Mienis, F., de Stigter, H.C., White, M., Duineveld, G., de Haas, H., van Weering, T.C.E., 2007. Hydrodynamic controls on cold-water coral growth and carbonate-mound development at the SW and SE Rockall Trough Margin, NE Atlantic Ocean. Deep Sea Research Part I: Oceanographic Research Papers 54, 1655-1674.

Millot, C., 1999. Circulation in the western Mediterranean Sea. Journal of Marine Systems 20, 423-442.

Millot, C., 2009. Another description of the Mediterranean Sea outflow. Progress in Oceanography 82, 101-124.

Millot, C., Taupier-Letage, I., 2005. Circulation in the Mediterranean Sea, in: Saliot, A. (Ed.), The Mediterranean Sea. Springer Berlin Heidelberg, pp. 29-66.

Morán, X.A.G., Estrada, M., 2001. Short-term variability of photosynthetic parameters and particulate and dissolved primary production in the Alboran Sea (SW Mediterranean). Marine Ecology Progress Series 212, 53-67.

Palomino, D., Vázquez, J.-T., Ercilla, G., Alonso, B., López-González, N., Díaz-del-Río, V., 2011. Interaction between seabed morphology and water masses around the seamounts on the Motril Marginal Plateau (Alboran Sea, Western Mediterranean). Geo-Marine Letters 31, 465-479.

Palomino D, Alonso B, Lo Iacono C, Casas D, d'Acremont E, Ercilla G, Gorini C, Vázquez J-T (2015) Seamounts and Seamount-like Structures of the Alborán Sea. In: Würtz M, Rovere M (eds) Atlas of the Mediterranean Seamounts and Seamount-like Structures. IUCN, Gland, Switzerland and Málaga, Spain, pp 21-58.

Patterson, R.T., Fishbein, E., 1989. Re-examination of the statistical methods used to determine the number of point counts needed for micropaleontological quantitative research. Journal of Paleontology 63, 245-248.

Pierre, C., 1999. The oxygen and carbon isotope distribution in the Mediterranean water masses. Marine Geology 153, 41-55.

Pomar, L., Morsilli, M., Hallock, P., Bádenas, B., 2012. Internal waves, an under-explored source of turbulence events in the sedimentary record. Earth-Science Reviews 111, 56-81.

Raddatz, J., Rüggeberg, A., Liebetrau, V., Foubert, A., Hathorne, E.C., Fietzke, J., Eisenhauer, A., Dullo, W.-C., 2014. Environmental boundary conditions of cold-water coral mound growth over the last 3 million years in the Porcupine Seabight, Northeast Atlantic. Deep Sea Research Part II: Topical Studies in Oceanography 99, 227-236.

Reimer, P.J., Bard, E., Bayliss, A., Beck, J.W., Blackwell, P.G., Bronk Ramsey, C., Buck, C.E., Cheng, H., Edwards, R.L., Friedrich, M., 2013. IntCal13 and Marine13 radiocarbon age calibration curves 0-50,000 years cal BP. Radiocarbon 55, 1869-1887.

Roberts, J., Wheeler, A., Freiwald, A., Cairns, S., 2009. Cold-water Corals: The Biology and Geology of Deep-Sea Coral Habitats. Cambridge University Press. 350 pp.

Roberts, J.M., Wheeler, A.J., Freiwald, A., 2006. Reefs of the deep: The biology and geology of cold-water coral ecosystems. Science 312, 543-547.

Rogerson, M., Cacho, I., Jimenez-Espejo, F., Reguera, M.I., Sierro, F.J., Martinez-Ruiz, F., Frigola, J., Canals, M., 2008. A dynamic explanation for the origin of the western Mediterranean organic-rich layers. Geochemistry, Geophysics, Geosystems 9, Q07U01.

Rüggeberg, A., Dullo, C., Dorschel, B., Hebbeln, D., 2007. Environmental changes and growth history of a cold-water carbonate mound (Propeller Mound, Porcupine Seabight). International Journal of Earth Sciences 96, 57-72.

Sarhan, T., Garcia Lafuente, J., Vargas, M., Vargas, J.M., Plaza, F., 2000. Upwelling mechanisms in the northwestern Alboran Sea. Journal of Marine Systems 23, 317-331.

Schmiedl, G., Pfeilsticker, M., Hemleben, C., Mackensen, A., 2004. Environmental and biological effects on the stable isotope composition of recent deep-sea benthic foraminifera from the western Mediterranean Sea. Marine Micropaleontology 51, 129-152.

Schmittner, A., Bostock, H.C., Cartapanis, O., Curry, W.B., Filipsson, H.L., Galbraith, E.D., Gottschalk, J., Herguera, J.C., Hoogakker, B., Jaccard, S.L., Lisiecki, L.E., Lund, D.C., Martínez-Méndez, G., Lynch-Stieglitz, J., Mackensen, A., Michel, E., Mix, A.C., Oppo, D.W., Peterson, C.D., Repschläger, J., Sikes, E.L., Spero, H.J., Waelbroeck, C., 2017. Calibration of the carbon isotope composition ($\delta^{13}C$) of benthic foraminifera. Paleoceanography 32, 512-530.

Sierro, F.J., Hodell, D.A., Curtis, J.H., Flores, J.A., Reguera, I., Colmenero-Hidalgo, E., Bárcena, M.A., Grimalt, J.O., Cacho, I., Frigola, J., Canals, M., 2005. Impact of iceberg melting on Mediterranean thermohaline circulation during Heinrich events. Paleoceanography 20.

Small, J., Martin, J., 2002. The generation of non-linear internal waves in the Gulf of Oman. Continental Shelf Research 22, 1153-1182.

Stalder, C., Vertino, A., Rosso, A., Ruggeberg, A., Pirkenseer, C., Spangenberg, J.E., Spezzaferri, S., Camozzi, O., Rappo, S., Hajdas, I., 2015. Microfossils, a key to unravel cold-water carbonate mound evolution through time: Evidence from the eastern Alboran Sea. PLoS One 10, e0140223.

Stalling, D., Westerhoff, M., Hege, H.-C., 2005. 38 - amira: A Highly Interactive System for Visual Data Analysis A2 - Hansen, Charles D, in: Johnson, C.R. (Ed.), Visualization Handbook. Butterworth-Heinemann, Burlington, pp. 749-767.

Stuiver, M., Reimer, P.J., 1993. Extended ^{14}C data base and revised CALIB 3.0 ^{14}C age calibration program. Radiocarbon 35, 215-230.

Stuut, J.-B., Smalley, I., O'Hara-Dhand, K., 2009. Aeolian dust in Europe: African sources and European deposits. Quaternary International 198, 234-245.

Taviani, M., Angeletti, L., Beuck, L., Campiani, E., Canese, S., Foglini, F., Freiwald, A., Montagna, P., Trincardi, F., 2016. Reprint of 'On and off the beaten track: Megafaunal sessile life and Adriatic cascading processes'. Marine Geology 375, 146-160.

Taviani, M., Vertino, A., Correa, M.L., Savini, A., De Mol, B., Remia, A., Montagna, P., Angeletti, L., Zibrowius, H., Alves, T., 2011. Pleistocene to Recent scleractinian deep-water corals and coral facies in the Eastern Mediterranean. Facies 57, 579-603.

Thierens, M., Browning, E., Pirlet, H., Loutre, M.F., Dorschel, B., Huvenne, V.A.I., Titschack, J., Colin, C., Foubert, A., Wheeler, A.J., 2013. Cold-water coral carbonate mounds as unique palaeo-archives: the Plio-Pleistocene Challenger Mound record (NE Atlantic). Quaternary Science Reviews 73, 14-30.

Titschack, J., Baum, D., De Pol-Holz, R., López Correa, M., Forster, N., Flögel, S., Hebbeln, D., Freiwald, A., Riegl, B., 2015. Aggradation and carbonate accumulation of Holocene Norwegian cold-water coral reefs. Sedimentology 62, 1873-1898.

Titschack, J., Fink, H.G., Baum, D., Wienberg, C., Hebbeln, D., Freiwald, A., 2016. Mediterranean cold-water corals - an important regional carbonate factory? The Depositional Record 2, 74-96.

Toucanne, S., Jouet, G., Ducassou, E., Bassetti, M.-A., Dennielou, B., Angue Minto'o, C.M., Lahmi, M., Touyet, N., Charlier, K., Lericolais, G., Mulder, T., 2012. A 130,000-year record of Levantine Intermediate Water flow variability in the Corsica Trough, western Mediterranean Sea. Quaternary Science Reviews 33, 55-73.

Van Rooij, D., Hebbelin, D., Comas, M., Vandorpe, T., Delivet, S., Nave, S., Michel, E., Lebreiro, S., Terrinha, P., Roque, C., 2013. MD 194/EUROFLEETS à bord du R/V Marion Dufresne. Cadix 10 juin 2013-Lisbonne 20 juin 2013.

Van Weering, T.C.E., de Haas, H., de Stigter, H.C., Lykke-Andersen, H., Kouvaev, I., 2003. Structure and development of giant carbonate mounds at the SW and SE Rockall Trough margins, NE Atlantic Ocean. Marine Geology 198, 67-81.

Vandorpe, T., Wienberg, C., Hebbeln, D., Van den Berghe, M., Gaide, S., Wintersteller, P., Van Rooij, D., 2017. Multiple generations of buried cold-water coral mounds since the Early-Middle Pleistocene Transition in the Atlantic Moroccan Coral Province, southern Gulf of Cádiz. Palaeogeography, Palaeoclimatology, Palaeoecology 485, 293-304.

Vargas-Yáñez, M., Plaza, F., Garcıa-Lafuente, J., Sarhan, T., Vargas, J., Vélez-Belchí, P., 2002. About the seasonal variability of the Alboran Sea circulation. Journal of Marine Systems 35, 229-248.

Victorero, L., Blamart, D., Pons-Branchu, E., Mavrogordato, M.N., Huvenne, V.A.I., 2016. Reconstruction of the formation history of the Darwin Mounds, N Rockall Trough: How the dynamics of a sandy contourite affected cold-water coral growth. Marine Geology 378, 186-195.

Wefing, A.-M., Arps, J., Blaser, P., Wienberg, C., Hebbeln, D., Frank, N., 2017. High precision U-series dating of scleractinian cold-water corals using an automated chromatographic U and Th extraction. Chemical Geology 475, 140-148.

Wheeler, A.J., Beyer, A., Freiwald, A., de Haas, H., Huvenne, V.A.I., Kozachenko, M., Olu-Le Roy, K., Opderbecke, J., 2007. Morphology and environment of cold-water coral carbonate mounds on the NW European margin. International Journal of Earth Sciences 96, 37-56.

Wheeler, A.J., Kozachenko, M., Beyer, A., Foubert, A., Huvenne, V.A.I., Klages, M., Masson, D.G., Olu-Le Roy, K., Thiede, J., 2005. Sedimentary processes and carbonate mounds in the Belgica Mound province, Porcupine Seabight, NE Atlantic, in: Freiwald, A., Roberts, J.M. (Eds.), Cold-Water Corals and Ecosystems. Springer Berlin Heidelberg, Berlin, Heidelberg, pp. 571-603.

White, M., Dorschel, B., 2010. The importance of the permanent thermocline to the cold water coral carbonate mound distribution in the NE Atlantic. Earth and Planetary Science Letters 296, 395-402.

White, M., Mohn, C., de Stigter, H., Mottram, G., 2005. Deep-water coral development as a function of hydrodynamics and surface productivity around the submarine banks of the Rockall Trough, NE Atlantic, in: Freiwald, A., Roberts, J.M. (Eds.), Cold-Water Corals and Ecosystems. Springer Berlin Heidelberg, Berlin, Heidelberg, pp. 503-514.

Wienberg, C., 2019. A deglacial cold-water coral boom in the Alboran Sea: from coral mounds and species dominance. In: Orejas C, Jiménez C, Mediterranean Cold-Water Corals: Past, Present and Future, Springer series: Coral Reefs of the World.

Wienberg, C., Frank, N., Mertens, K.N., Stuut, J.-B., Marchant, M., Fietzke, J., Mienis, F., Hebbeln, D., 2010. Glacial cold-water coral growth in the Gulf of Cádiz: Implications of increased palaeo-productivity. Earth and Planetary Science Letters 298, 405-416.

Wienberg, C., Titschack, J., 2017. Framework-Forming Scleractinian Cold-Water Corals Through Space and Time: A Late Quaternary North Atlantic Perspective, in: Rossi, S., Bramanti, L., Gori, A., Orejas Saco del Valle, C. (Eds.), Marine Animal Forests: The Ecology of Benthic Biodiversity Hotspots. Springer International Publishing, Cham, pp. 699-732.

Wienberg, C., Titschack, J., Freiwald, A., Frank, N., Lundälv, T., Taviani, M., Beuck, L., Schröder-Ritzrau, A., Krengel, T., Hebbeln, D., 2018. The giant Mauritanian cold-water coral mound province: Oxygen control on coral mound formation. Quaternary Science Reviews 185, 135-152.

Zahn, R., Winn, K., Sarnthein, M., 1986. Benthic foraminiferal $\delta^{13}C$ and accumulation rates of organic carbon: *Uvigerina peregrina* group and *Cibicidoides wuellerstorfi*. Paleoceanography 1, 27-42.

Table 1. Metadata of gravity cores collected in the WMCP (southern Alboran Sea) during the cruise MD 194 “GATEWAY” with the French RV Marion Dufresne and cruise MSM 36 “MoccoMeBo” with the German RV Maria S. Merian.

Cruise	Core Type	Core ID	Latitude [N]	Longitude [W]	Water depth [m]	Recovery [cm]
MD194	On-mound	MD13-3451G	35°29.996′	3°02.398′	370	522
MD194	On-mound	MD13-3452G	35°28.128′	3°04.661′	305	558
MSM-36	On-mound	GeoB18127-1	35°28.969′	3°04.641′	365	563
MSM-36	On-mound	GeoB18130-1	35°28.099′	3°08.747′	379	148
MSM-36	Off-mound	GeoB18131-1	35°28.093′	3°09.301′	457	851

Table 2. AMS ^{14}C dates obtained from CWC fragments collected from the on-mound cores MD13-3451G and MD13-3452G. The ages were corrected for ^{13}C and a reservoir age of 400 years. The AMS ^{14}C ages were converted into calendar age with the CALIB 7.10 (Stuiver and Reimer, 1993; http://calib.org/calib/calib.html), using the MARINE-13 curve (Reimer et al., 2013). Coral mound aggradation rates (ARs) are calculated based on a linear interpolation of the coral ages.

Core ID (MD13-)	Core Depth [cm]	Lab-code	Coral Species	Conventional Age [kyr]		2σ range cal. age [kyr BP P=AD 1950]		Median Probability Age [kyr BP]	AR [cm kyr^{-1}]
				^{14}C age	± error				
3451G	5	Poz-62332	*M. oculata*	4.37	0.03	4.41	4.61	4.51	-
3451G	197	Poz-62333	*L. pertusa*	8.90	0.04	9.47	9.66	9.54	38.1
3451G	382	Poz-62334	*L. pertusa*	10.39	0.05	11.24	11.74	11.47	96.3
3451G	488	Poz-62335	*L. pertusa*	12.32	0.05	13.63	13.95	13.79	45.5
3452G	13	Poz-62336	*M. oculata*	3.58	0.03	3.38	3.56	3.47	-
3452G	99	Poz-62337	*M. oculata*	8.61	0.04	9.13	9.40	9.28	14.8
3452G	203	Poz-62338	*M. oculata*	9.11	0.05	9.66	10.09	9.85	181.8
3452G	267	Poz-62339	*L. pertusa*	9.90	0.04	10.70	11.02	10.85	63.6
3452G	355	Poz-62340	*M. oculata*	11.45	0.05	12.75	13.08	12.91	42.7
3452G	406	Poz-62341	*L. pertusa*	11.83	0.07	13.16	13.44	13.30	131.8
3452G	467	Poz-62342	*L. pertusa*	12.17	0.05	13.46	13.78	13.62	191.8
3452G	550	Poz-62343	*L. pertusa*	12.54	0.05	13.87	14.16	14.02	204.9

Table 3. U/Th dates, uranium and thorium isotope concentrations and ratios obtained from CWC fragments collected from the on-mound cores GeoB18127-1 and GeoB18130-1 (n.d. not determinable). Coral mound aggradation rates (ARs) are calculated based on a linear interpolation of the coral ages.

Core ID [GeoB]	Core Depth [cm]	Lab-code	Coral Species	Age [kyr BP]	± [kyr]	^{238}U [ppm]	± [ppm]	^{232}Th [ppb]	± [ppb]	$\delta^{234}U_0$ [‰]	error	AR [cm kyr^{-1}]
18127-1	1	IUP-7734	*M. oculata*	5.39	0.12	4.218	0.0006	0.282	0.009	150.5	2.7	-
18127-1	15	IUP-7735	*M. oculata*	5.76	0.09	4.233	0.0005	n.d.		146.9	3.1	37.2
18127-1	52	IUP-7736	*L. pertusa*	7.56	0.20	3.362	0.0007	n.d.		150.3	3.0	20.5
18127-1	79	IUP-7737	*M. oculata*	*#7.81*	0.16	4.122	0.0005	0.101	0.006	149.5	2.6	-
18127-1	79	IUP-7738	*L. pertusa*	*#8.23*	0.14	3.445	0.0004	0.199	0.007	149.4	3.1	40.4
18127-1	90	IUP-7739	*L. pertusa*	8.30	0.12	3.182	0.0004	0.057	0.002	149.3	3.0	158.3
18127-1	159	IUP-7740	*L. pertusa*	8.55	0.12	4.168	0.0005	0.622	0.010	150.7	2.8	-
18127-1	189	IUP-7741	*L. pertusa*	8.51	0.17	3.921	0.0005	0.229	0.007	151.9	3.4	479.0
18127-1	252	IUP-7742	*L. pertusa*	9.28	0.14	3.234	0.0004	n.d.		148.2	2.7	82.0
18127-1	274	IUP-7743	*L. pertusa*	9.70	0.08	3.659	0.0004	0.091	0.002	149.3	2.6	51.7
18127-1	337	IUP-7744	*L. pertusa*	10.35	0.09	3.420	0.0003	0.179	0.002	143.3	2.5	97.7
18127-1	373	IUP-7745	*L. pertusa*	11.14	0.07	4.177	0.0003	0.293	0.002	145.8	1.9	45.2
18127-1	404	IUP-7746	*L. pertusa*	13.30	0.10	3.398	0.0002	0.354	0.002	149.8	2.1	14.4
18127-1	460	IUP-7747	*L. pertusa*	13.40	0.10	3.712	0.0002	0.224	0.002	148.7	1.4	546.9
18127-1	478	IUP-7748	*L. pertusa*	13.45	0.09	3.758	0.0002	0.323	0.002	149.6	2.2	335.2
18127-1	491	IUP-7749	*L. pertusa*	14.07	0.11	3.288	0.0002	0.362	0.002	148.9	1.5	20.2
18130-1	2	IUP-7750	*M. oculata*	5.28	0.04	4.514	0.0003	0.166	0.001	146.8	2.0	-
18130-1	9	IUP-7751	*M. oculata*	**5.00*	0.03	3.989	0.0002	0.050	0.000	149.9	1.8	-
18130-1	34	IUP-7752	*M. oculata*	7.88	0.05	3.957	0.0002	0.256	0.002	148.6	1.4	12.4
18130-1	61	IUP-7753	*M. oculata*	8.41	0.06	3.773	0.0003	0.136	0.001	148.1	1.9	51.0
18130-1	71	IUP-7754	*L. pertusa*	8.83	0.05	4.062	0.0002	0.387	0.001	149.5	0.9	23.6
18130-1	106	IUP-7755	*L. pertusa*	8.88	0.04	3.506	0.0002	0.232	0.001	149.1	0.9	704.2
18130-1	118	IUP-7756	*M. oculata*	9.07	0.05	3.735	0.0002	0.334	0.002	147.7	0.9	63.1
18130-1	128	IUP-7757	*L. pertusa*	9.40	0.05	3.483	0.0002	0.713	0.003	149.3	1.1	
18130-1	138	IUP-7758	*L. pertusa*	9.38	0.05	3.851	0.0002	0.627	0.002	149.1	0.9	> 270
18130-1	147	IUP-7759	*L. pertusa*	9.37	0.05	4.131	0.0002	0.306	0.001	148.9	1.4	

*: age reversal. #: two different ages obtained from *L. pertusa* and *M. oculata* at the same core depth, see text for explanation.

Table 4. AMS ^{14}C dates of mixed planktonic foraminifers obtained from the off-mound core GeoB18131-1. The ages were corrected for ^{13}C and a reservoir age of 400 years. The AMS ^{14}C ages were converted into calendar age with the CALIB 7.10 (Stuiver and Reimer, 1993; http://calib.org/calib/calib.html), using the MARINE-13 curve (Reimer et al., 2013). Below 400 cm core depth, the age model is based on visual tie-point correlation between the $\delta^{18}O$ record of core GeoB18131-1 and the LR04 $\delta^{18}O$ stack record (Lisiecki and Raymo, 2005). Sedimentation rates are calculated based on a linear interpolation of the AMS ^{14}C dates and tie points.

Core ID [GeoB]	Core Depth [cm]	Lab-code	Conventional Age: ^{14}C age [kyr]	Conventional Age: ± error [kyr]	2σ range cal. age [kyr BP P=AD 1950]		Median Probability Age [kyr BP]	Sedimentation Rate [cm kyr^{-1}]
18131-1	3	Poz-84167	0.63	0.03	0.189	0.376	0.3	-
18131-1	168	Poz-84348	7.84	0.05	8.183	8.394	8.3	20.5
18131-1	193	Poz-84349	9.49	0.05	10.217	10.484	10.3	12.3
18131-1	198	Poz-84350	9.74	0.05	10.506	10.793	10.6	16. 5
18131-1	273	Poz-84351	17.50	0.1	20.335	20.913	20.6	7.5
18131-1	363	Poz-84300	20.27	0.32	23.040	24.697	23.9	27.5
Core ID [GeoB]	Core Depth [cm]						Tie-Point Age [kyr BP]	Sedimentation Rate [cm kyr^{-1}]
18131-1	423	Tie points to the LR04 $\delta^{18}O$ stack record (Lisiecki & Raymo, 2005)					32	7.4
18131-1	608						52.5	9.0
18131-1	708						68	6.5
18131-1	758						80	4.2
18131-1	768						82	3.0
18131-1	848						110	2.9

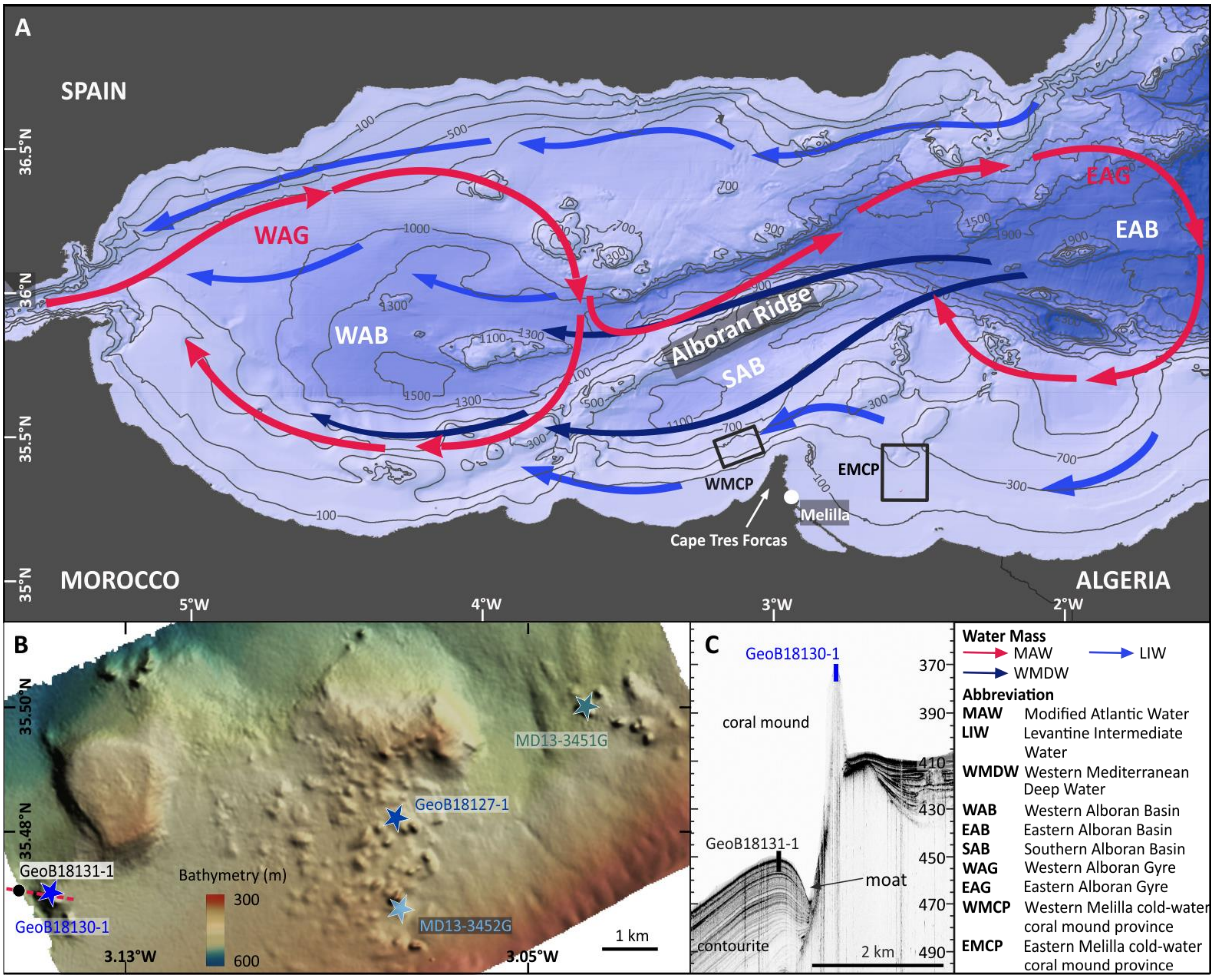

Figure 1. (**A**) Bathymetry map of the Alboran Sea (western Mediterranean Sea) (Map: Marine Information Service (2016); EMODnet Digital Bathymetry, http://doi.org/10.12770/c7b53704-999d-4721-b1a3-04ec60c87238). Displayed is the schematic present-day oceanic circulation pattern in the Alboran Sea. Two black rectangles represent the West Melilla cold-water coral mound province (WMCP; this study) and the East Melilla cold-water coral mound province (EMCP). (**B**) Shaded relief map of the WMCP showing the location of the four on-mound cores (stars; MD13-3451G, MD13-3452G, GeoB18127-1, and GeoB18130-1) and one off-mound core (dot; GeoB18131-1) presented in this study. (**C**) Sub-bottom profile (parasound) from the WMCP (modified after Hebbeln et al., 2009) indicating the sampling sites of the on-mound core GeoB18130-1 and the off-mound core GeoB18131-1. The location of the cross profile is indicated as a red dashed line in (B).

1080

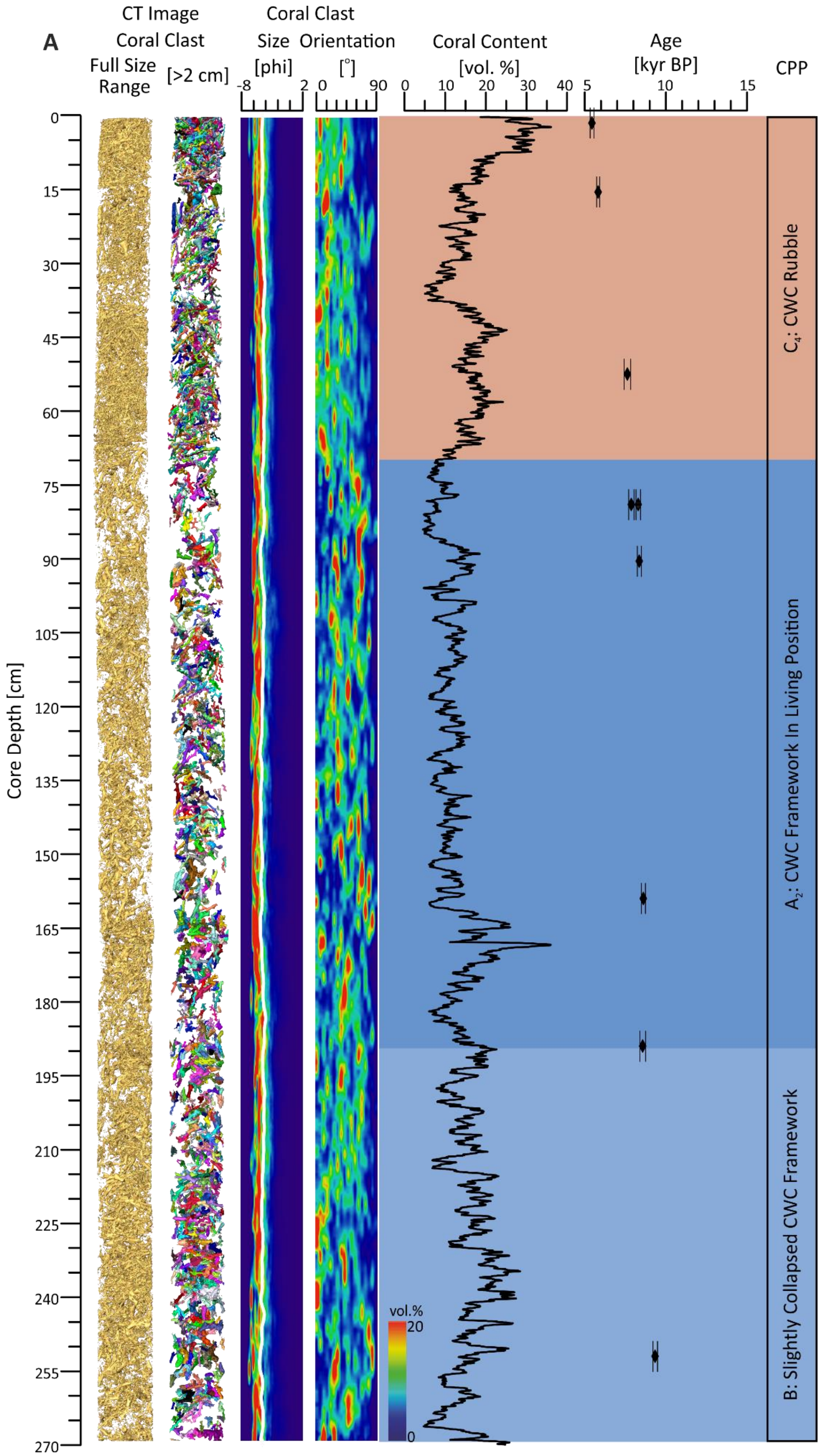

A
CT Image
Coral Clast
Full Size Range
[>2 cm]
Coral Clast
Size [phi]
-8 2
Orientation [°]
0 90
Coral Content [vol. %]
0 10 20 30 40
Age [kyr BP]
5 10 15
CPP
Core Depth [cm]
0
15
30
45
60
75
90
105
120
135
150
165
180
195
210
225
240
255
270
vol.%
20
0
C4: CWC Rubble
A2: CWC Framework In Living Position
B: Slightly Collapsed CWC Framework

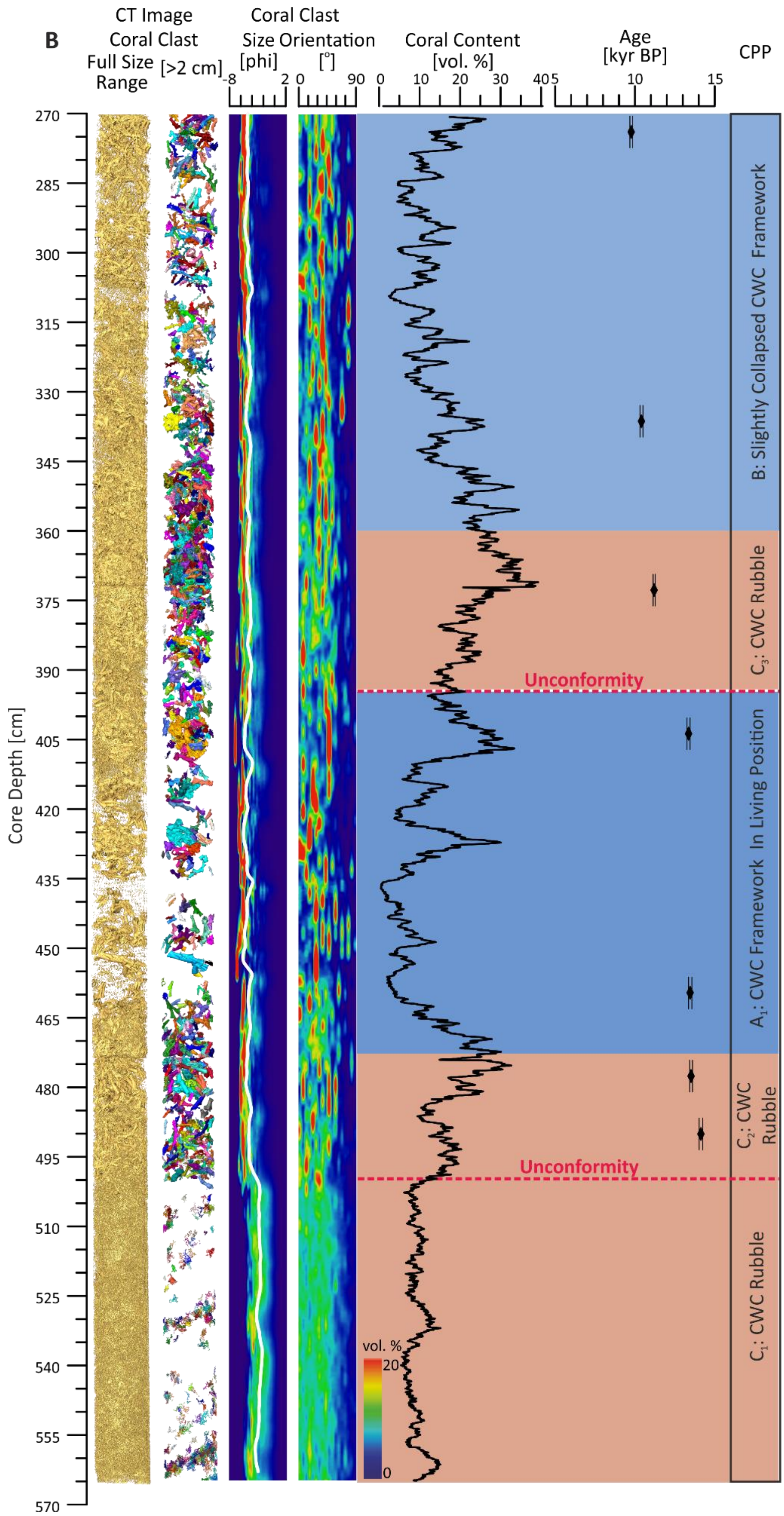
B
CT Image
Full Size Range
Coral Clast [>2 cm]
Coral Clast
Size [phi]
-8 2
Orientation [°]
0 90
Coral Content [vol. %]
0 10 20 30 40
Age [kyr BP]
5 10 15
CPP
Core Depth [cm]
270
285
300
315
330
345
360
375
390
405
420
435
450
465
480
495
510
525
540
555
570
B: Slightly Collapsed CWC Framework
C3: CWC Rubble
Unconformity
A1: CWC Framework In Living Position
C2: CWC Rubble
Unconformity
C1: CWC Rubble
vol. %
20
0

Figure 2. Log of the on-mound core GeoB18127-1 (**A**: 0-269 cm, **B**: 270-563 cm core depth) retrieved from a coral mound of the West Melilla cold-water coral mound province. From left to right: Core CT 3D image of coral clast in full size range, coral clast larger than >2 cm, coral clast size distribution (white line indicates the mean clast size), coral clast orientation, quantified coral content based on the CT data, and U-series coral ages. Three different cold-water coral (CWC) preservation patterns (CPPs) were recognized. CPP A: CWC framework in living position (highlighted by blue shading), CPP B: slightly collapsed CWC framework (highlighted by light blue shading), and CPP C, CWC rubble (highlighted by light red shading). Red dashed lines represent two unconformities identified at core depths of 500 cm and 395 cm.

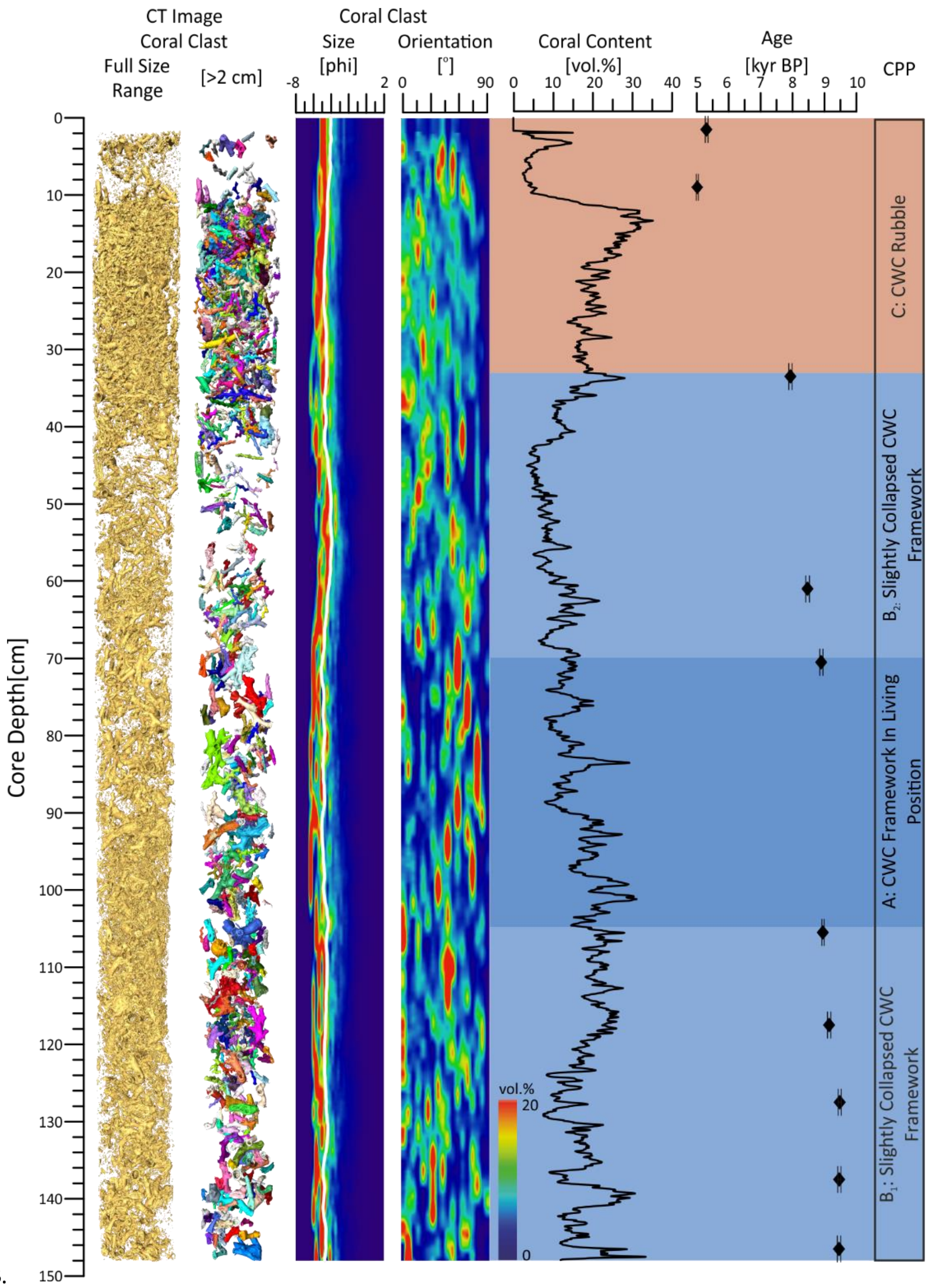

Figure 3. Log of the on-mound core GeoB18130-1 (0-148 cm core depth) collected from a coral mound in the West Melilla cold-water coral mound province. From left to right: Core CT 3D image of coral clast in full size range, coral clast large than >2 cm, coral clast size distribution (white line indicates the mean clast size), coral clast orientation, quantified coral content based on the CT data, and U-series coral ages. Three different cold-water coral (CWC) preservation patterns (CPPs) were recognized. CPP A: CWC framework in living position (highlighted by blue shading), CPP B: slightly collapsed CWC framework (highlighted by light blue shading), and CPP C: CWC rubble (highlighted by light red shading).

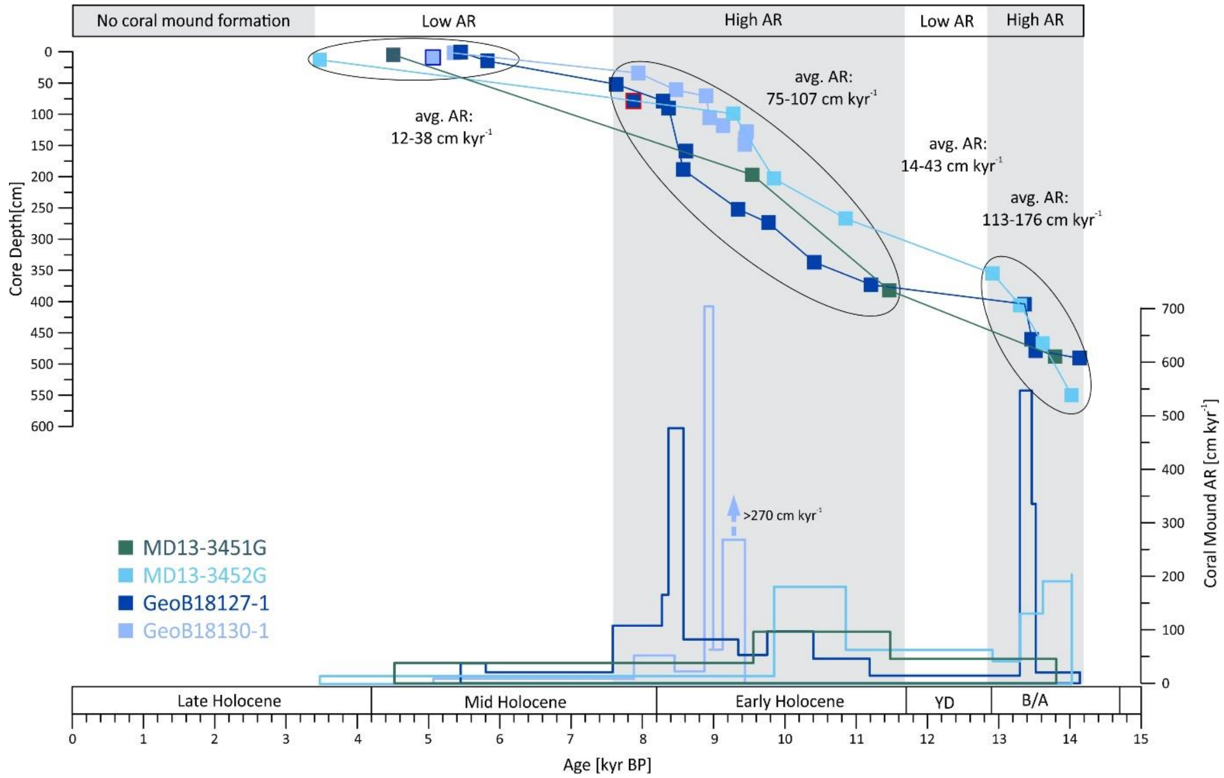

Figure 4. Cold-water coral (CWC) ages (filled squares) versus core depth and corresponding calculated coral mound aggradation rates (ARs) of four on-mound cores collected in the West Melilla cold-water coral mound province (WMCP, see legend for core-ID and color code). Filled square with blue frame indicates an age reversal and filled square with red frame indicates an age obtained from *Madrepora oculata*, both of which were not used for the calculation of ARs (see text for explanation). The CWC ages cluster in three periods, which mainly correspond to the Bølling-Allerød (B/A) interstadial, the Early Holocene and the Mid Holocene (highlighted by ovals). During the B/A and the Early Holocene, highest ARs are obtained with average (avg.) values ranging between 75 and 176 cm kyr^{-1}. During the Younger Dryas (YD), the avg. ARs decreased to 14-43 cm kyr^{-1}. In the Mid Holocene, the avg. ARs range between 12 and 38 cm kyr^{-1}. Since the onset of the Late Holocene, mound formation in the WMCP seems to stagnate. The B/A, the YD and the sub-periods of the Holocene are temporally defined according to Walker et al. (2012) and Lowe et al. (2008).

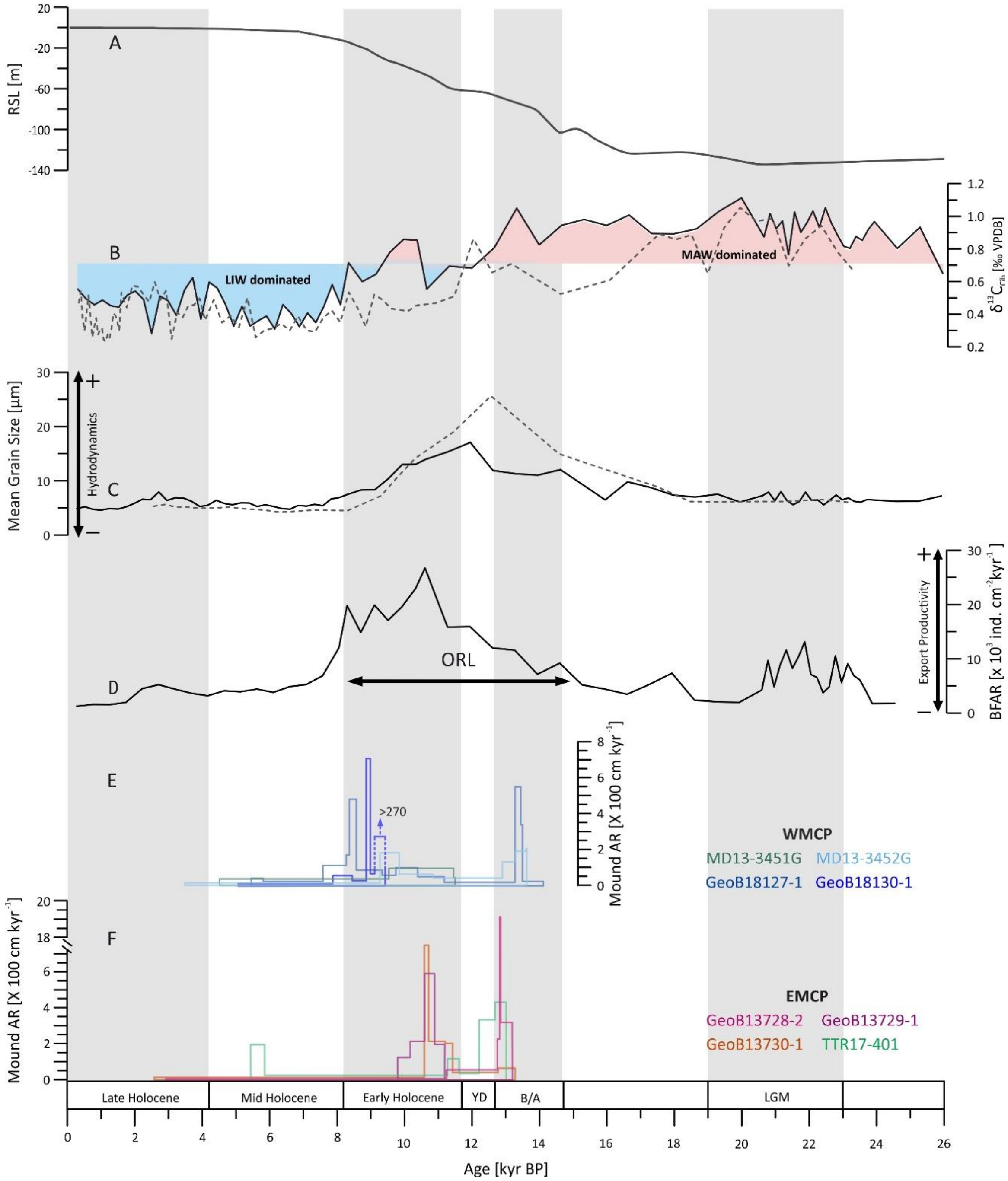

Figure 5. Compilation of paleoceanographic multi-proxy data obtained from the off-mound core GeoB18131-1 collected in the West Melilla cold-water coral mound province (WMCP) focusing on the past 26 kyr supplemented by other paleoceanographic records. (**A**) Relative Sea Level (RSL) record (Lambeck et al., 2014). (**B**) $\delta^{13}C_{Cib}$ records of mixed benthic foraminifers (*Cibicidoides mundulus* and *Cibicidoides pachyderma*) obtained for the WMCP (black line; this study) and of *Cibicidoides kullenbergi* obtained for the East Melilla cold-water coral mound province (EMCP; grey dashed line; Fink et al., 2013) used as a proxy for water column structure. Pink shading indicates a dominance of the Modified Atlantic Water (MAW) during the last glacial, while light blue shading marks a dominance of the Levantine Intermediate Water (LIW) since the Mid Holocene. (**C**) Mean grain size used as proxy for bottom current strength (WMCP: black line, this study; EMCP: grey dashed line, Fink et al., 2013). (**D**)

Benthic foraminifera accumulation rate (BFAR) record obtained from the WMCP and used as a proxy for export productivity. (**e-F**) Cold-water coral mound aggradation rates (ARs) obtained from various on-mound cores collected from (**E**) the WMCP (this study) and (**F**) the EMCP (Fink et al., 2013; Stalder et al., 2015). The Last Glacial Maximum (LGM) and rapid events during the deglaciation (B/A: Bølling-Allerød, YD: Younger Dryas) and sub-periods of the Holocene are temporally defined according to Walker et al. (2012) and Lowe et al. (2008). MIS: Marine Isotope Stage.

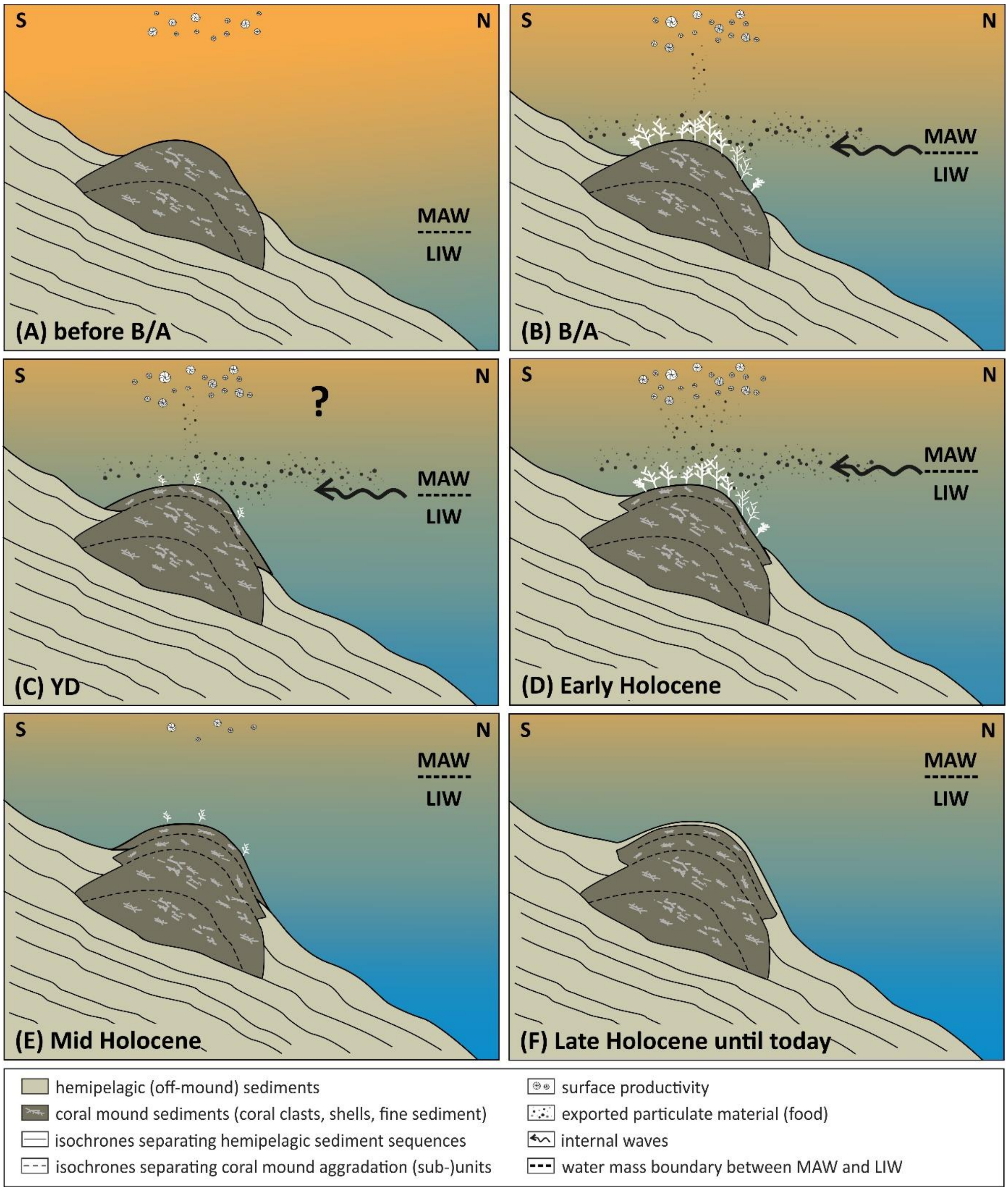

Figure 6. Schematic model showing the chronology of coral mound formation for the West Melilla cold-water coral mound province (WMCP) since the last deglaciation. The blue/green-colored water column represents a predominance of the westward-flowing Levantine Intermediate Water (LIW) in the depth level of coral mound occurrence, while the yellow/orange shading indicates a predominance of the eastward-flowing Modified Atlantic Water (MAW). Curved arrow indicates internal waves that develop due to enhanced interactions at the interface between the MAW and the LIW. (**A**) Before the Bølling-Allerød (B/A) interstadial: Coral mounds of the WMCP were in a dormant state. (**B**) B/A interstadial: Enhanced coral mound formation. The interface between the MAW and the LIW were placed towards the coral mounds. Internal waves that likely developed along this

interface (indicated by enhanced bottom current strength) promoted increased delivery of food particles to the CWCs. At the same time, increased sea surface productivity also contributed to the enhanced export of particulate material. (**C**) Younger Dryas (YD): Temporary slow-down of coral mound formation despite overall optimal environmental conditions for CWC growth. (**D**) Early Holocene to early Mid-Holocene: Enhanced coral mound formation. Similar environmental conditions prevailed as indicated for the B/A interstadial. (**E**) Mid Holocene: Slow-down of coral mound formation. Coral mounds became submerged by the LIW and a relatively stable hydrodynamic setting was established. Surface and export productivity significantly decreased. (**F**) Late Holocene until present. CWCs completely declined, mound formation stagnated and some coral mounds in the WMCP became buried by sediments.